JANUARY 1976 MATT-1180



# FUSION REACTIVITIES AND NEUTRON SOURCE CHARACTERISTICS OF BEAM-DRIVEN TOROIDAL REACTORS WITH BOTH D AND T INJECTION

BY

D. L. JASSBY AND H. H. TOWNER

## PLASMA PHYSICS LABORATORY


PRINCETON UNIVERSITY
PRINCETON, NEW JERSEY

This work was supported by U. S. Energy Research and Development Administration Contract E(11-1)-3073. Reproduction, translation, publication, use and disposal, in whole or in part, by or for the United States Government is permitted.

## DISCLAIMER

NOTICE



Printed in the United States of America.

Available from
National Technical Information Service
U. S. Department of Commerce
5285 Port Royal Road
Springfield, Virginia 22151
Price: Printed Copy $ * ; Microfiche $1.45

| *Pages | NTIS Selling Price |
|---|---|
| 1-50 | $ 4.00 |
| 51-150 | 5.45 |
| 151-325 | 7.60 |
| 326-500 | 10.60 |
| 501-1000 | 13.60 |

# FUSION REACTIVITIES AND NEUTRON SOURCE CHARACTERISTICS OF BEAM-DRIVEN TOROIDAL REACTORS WITH BOTH D AND T INJECTION

D. L. JASSBY, H. H. TOWNER

Plasma Physics Laboratory, Princeton University
Princeton, New Jersey 08540, U.S.A.



## ABSTRACT

We consider the reactor performance of intensely beam-driven tokamak plasmas with 50:50 D-T composition maintained by neutral-beam injection of both D and T, together with plasma recycling. The D and T are injected with equal intensity and velocity. This mode of operation is most appropriate for high-duty-factor, high-power-density operation, in the absence of pellet injection.

The isotropic velocity distributions of energetic D and T ions (for multi-angle injection) are calculated from a simple slowing-down model, but include a tail above the injection velocity. The neutron source characteristics are determined from fusion reactivities calculated for beam-target, hot-ion, and thermonuclear reactions. For conditions where $Q \sim 1$, beam-target reactions are dominant, although reactions among the hot ions contribute substantially to $P_{fusion}$ when $n_{hot}/n_e \gtrsim 0.2$.

For given values of injection energy $W_o$, plasma radius $a_p$, and $n_{hot}/n_e$, $P_{fusion}$ has a maximum in $n_e\tau_E$ (which determines $T_e \simeq T_i$), and therefore in Q. Suitable

conditions for many applications are $W_o \sim 200$ keV, $T_e \approx T_i \approx 8$ keV, and $0.1 \lesssim n_{hot}/n_e \lesssim 0.3$, for which $Q = 0.7$ to 1.0 and $n_e\tau_E = 0.6$ to $2\times10^{13}$ $cm^{-3}s$. The larger values of $n_{hot}/n_e$ yield the largest neutron wall loading, $\phi_w$, for given-sized devices, permit a smaller $W_o$ for a given $P_{fusion}$ or $\phi_w$, and demand the smallest $n_e\tau_E$. When $n_e a_p$ is limited both by adequate neutral-beam penetration and by the MHD pressure limitation, then $\phi_w$ increases slightly faster than linearly with both maximum magnetic field (at the coils) and plasma vertical elongation, and can reach 4 $MW/m^2$ with $B_M = 140$ kG and elongation = 3.

# 1. INTRODUCTION

Beam-driven D-T toroidal fusion reactors have been discussed in a number of recent papers [1,2]. Large values of Q = (fusion power production/injected beam power) are attainable provided that $n\tau_E$, the product of density and energy confinement time, is sufficiently large ($> 5\times10^{13}$ $cm^{-3}s$). On the other hand, the maximum attainable fusion power density, $P_f$, tends to occur at relatively modest values of $n\tau_E$, where Q is of order unity [3]. There are a number of potential reactor applications where a large production rate of 14-MeV neutrons at Q~1 is desirable: fusion engineering test facilities [4], the breeding of fissile fuel [3], fusion-fission hybrid reactors [5-7], and the burning of long-lived actinide wastes [7]. For these applications, economic considerations tend to favor the maximization of $P_f$ and the related quantity, neutron wall loading, since the cost of 14-MeV neutrons from the reactor is roughly inversely proportional to $P_f$. Nevertheless, it is also important that Q be larger than about 0.5, since the required investment in neutral-beam injectors, and the quantities of electrical power and tritium that must be circulated, are nearly inversely proportional to Q.

The low-$n\tau_E$, high-$P_f$ regime is often referred to as TCT (two-energy-component torus) operation. Ideal TCT performance is realized in the case of a pure tritium plasma whose temperature is sustained by Coulomb energy transfer from injected superthermal deuterons [1-3]. However, maintaining a highly enriched tritium plasma in the face of continuous deuteron injection is a formidable problem, and probably requires the continuous injection of

tritium pellets. In the absence of pellet injection technology, the optimal tritium strategy, which is discussed in Section 2, appears to consist of treating the deuteron and triton plasma components in a perfectly symmetric manner. That is, $D^o$ and $T^o$ beams are injected with the same velocity, and with sufficient intensity to maintain a 50:50 D-T bulk plasma - which is fueled by the injected beams together with plasma recycling. The values of Q and $P_f$ are necessarily smaller than those attainable in the ideal D-on-T situation, although significant fusion power is also produced from thermonuclear reactions, and especially from reactions among the energetic D and T ions themselves. In the limiting case where the superthermal-ion density becomes a large fraction of the electron density, one approaches a class of reactors, such as the CBT or CIT ( counterstreaming-ion torus ) [8-10], which can provide large Q and $P_f$ in relatively small toroidal devices.

This paper presents the fusion reactivities, power multiplication, power outputs, and neutron wall loadings for 50:50 D-T toroidal plasmas maintained by injection of energetic D and T neutral beams, for wide ranges of injected energy and relative superthermal-ion density. Particular account is taken of fusion reactions among the energetic D and T ions. While most of this work applies to any low-to-moderate-beta toroidal reactor, we consider specifically tokamak devices. Section 2 of this paper presents the rationale for 50:50 D-T systems. Section 3 describes the velocity distributions that are used in Section 4 to calculate fusion reactivities among the various D and T plasma components. These reactivities are then employed to calculate Q, $P_f$, and other neutron source

characteristics. Section 5 presents Q-values for 50:50 D-T systems, as a function of relative energetic-ion density. The corresponding fractional tritium burn-ups are given in Section 6. (This latter quantity determines the required capacity of the tritium processing system, as well as the required plant tritium inventory.) Section 7 describes how the fusion power output and neutron wall loading vary with plasma parameters, including neutral-beam energy, plasma elongation, and magnetic field strength. The plasma density is constrained either by the requirement of adequate neutral-beam penetration, or by the MHD limit on the total plasma pressure. The maximum attainable neutron wall loading is investigated using two approaches, the first employing fixed aspect ratio, and the second specifying a fixed distance from the major axis to the inner edge of the plasma. Section 8 presents the conclusions.

## 2. TRITIUM STRATEGIES FOR BEAM-DRIVEN TOROIDAL REACTORS

### 2.1 D→T COMPARED WITH T→D

In the design of TCT-type reactors, the question arises whether to inject deuteron beams into a tritium target plasma (D→T), or vice versa (T→D). This question can be answered by considering relative values of Q, $P_f$, and fractional tritium burn-up. Figure 1 shows Q as a function of injection energy $W_o$ and bulk-plasma temperature $T_e = T_i$, for both D→T and T→D. (These calculations use the energetic-ion slowing-down formulation of Reference [11].) As expected, the T→D Q-values peak at injection energies ≃ 50% larger than the optimum energies for D→T, that is, where the injected velocities are nearly the same. For typical plasma

temperatures (5-10 keV), the T→D Q-values are about 20% smaller. (At very low $T_e$, electron drag is dominant, and the 50% greater investment in $W_o$ for T→D is balanced by the 50% larger slowing-down time. At large $T_e$, ion drag becomes important, and the energy slowing-down rate on background ions is 50% larger for T→D than for D→T. In the limit of very large $T_e$, $Q_{T\to D} = 2/3\ Q_{D\to T}$.)

If a target plasma of given $n_e$, $T_e$, and $\tau_E$ is heated solely by injected beams, then $P_f \propto Q$, so that maximum $P_f$ in the T→D case is typically lower than for D→T by about 20% - if there is no restriction on plasma pressure. The pressure of the energetic-ion component in the T→D case is about 20% larger. If, as seems likely, the plasma pressure is always to be maintained at the maximum allowed by MHD equilibrium, then both $n_e$ and $P_b$ must be reduced by about 10% in the T→D case, for typical systems where beam pressure ~ bulk-plasma pressure [3]. The result is a further 20% decrease in $P_f$. Summarizing, for T→D, maximum Q is about 20% lower, and $P_f$ may be 35% lower than the maximum values for D→T.

Now let us consider the tritium burn-up rate. For large-$P_f$ reactors, we have $\tau_s \gtrsim \tau_E$, where $\tau_s$ is the fast-ion slowing-down time, and $n_{hot}/n_e \gtrsim 1/10$ [3]. If $\tau_p$ is the ion lifetime in the thermal plasma, we have, typically, $\tau_p \gtrsim 3\tau_E$ [12]. (Note that $\tau_E$ includes <u>all</u> transport, radiation, and charge-exchange losses.) Defining $F_b$ as the fractional burn-up of tritium per pass, then for reactors of the same power output,

$$\frac{F_{b,T\to D}}{F_{b,D\to T}} \approx \frac{n_e}{\tau_p}\left(\frac{n_{hot}}{\tau_s}\right)^{-1} \sim 3 \qquad (1)$$

That is, when the tritons are injected via beams, and removed from the machine immediately after thermalization, the burn-up per pass is about 3 times larger than the case where the tritons are injected (by pellets or gas) to form the target plasma. Thus the T→D mode could be advantageous, depending on the difficulties of handling large quantities of tritium, and the need to minimize the total tritium inventory.

For either of these operating modes, dilution of the target species by the beam species must be avoided to obtain maximum performance. Resolving this problem leads to several less ideal modes of operation, which are discussed in the following.

## 2.2 METHODS OF TRITIUM FUELING

We can differentiate various modes of operation of a beam-driven DT reactor, according to the means by which tritium fueling is carried out. We are concerned especially with plasmas of only moderate $n_e\tau_E$-values, typically less than $3 \times 10^{13}$ $cm^{-3}s$. In describing the following practical options for tritium fueling, we consider how Q and $P_f$ are likely to be reduced from the maximum values attained in the ideal D→T mode.

2.2.1 Pellet injection of tritium. The tritium background plasma can be maintained against particle loss by injecting high-velocity pellets [13] or clustres [14]. As before, we assume that $\tau_s \gtrsim \tau_E$, and $\tau_p \sim 3\tau_E$. The lifetime of thermalized deuterons should be approximately $\tau_p - \tau_s$, since there is a gradual diffusion outward of fast deuterons during slowing-down. If plasma recycling can be eliminated, in steady state the fraction of deuterons among the thermal ions is

$$\frac{n_D}{n_T}(\text{thermal}) = \frac{n_{hot}}{n_T}\,\frac{\tau_p - \tau_s}{\tau_s} \gtrsim \frac{1}{5} \qquad (2)$$

Taking into account bulk-plasma thermonuclear reactions, both Q and $P_f$ will be reduced by at least 16%. Attaining this performance demands that all escaping ions be removed from the torus by means of an unload divertor [15], with zero recycling coefficient, in order to avoid a further increase in $n_D/n_T$. Therefore, this method requires perfection of both pellet and magnetic divertor technologies.

2.2.2 Pulsed operation. Cyclic operation is possible in which the torus is filled with tritium at the beginning of each cycle, no tritium fueling is carried out during the power pulse, and no divertor is employed. As the injected deuterons thermalize with the target plasma, $n_e$ gradually increases, and $T_e$ decreases, unless the beam power is increased during the pulse. The gas pressure outside the plasma may quickly rise to a level that interferes with neutral beam transmission. (Typically, $5 \times 10^{21}$ atoms/s are injected into the torus.) If $P_b$ is constant, then in ten slowing-down times, the bulk-plasma is about 50:50 D-T, while $T_e$ is significantly reduced, so that Q and $P_f$ are reduced by a factor of at least 3. For $n_e \sim 5 \times 10^{13}$ cm$^{-3}$, $T_e \sim 6$ keV, $n_e\tau_E \sim 10^{13}$ cm$^{-3}$s, the useful pulse time is 2 to 3 s. (Increasing $P_b$ during the pulse does not significantly change this result.) The plasma current is then terminated, the vacuum vessel exhausted, and the torus refilled with tritium. The duty factor probably cannot exceed 20%, so that it is unlikely that this operation could be

economically viable. Further serious problems are the thermal cycling experienced by the blanket and vacuum wall, and the energy storage required between cycles. (Actually, it may not be necessary to shut down the plasma current, if the gas charge can be purified between power pulses by admitting tritium and simultaneously pumping for an extended period.)

2.2.3 Gas injection of tritium. In principle, the tritium can be fueled during the power pulse by means of a dense tritium blanket surrounding the plasma [16]. The inward diffusion of cold plasma (a somewhat mysterious process) would bring fuel into the reacting region. But this method would also encourage particle recycling, so that the fraction of deuterons in the bulk plasma would build up to a larger value than in the pellet-fueled case, and the plasma density might reach intolerably high levels during long pulses. The density-thickness product of the cold blanket region must be relatively small ($< 10^{15}$ cm$^{-2}$), in order to permit beam penetration to the reacting region of the torus, while the gas pressure in the beam ducts must be maintained at less than $3 \times 10^{-5}$ torr.

2.2.4 Low-voltage beam injection. The plasma tritium content can be fueled by low-voltage beams [6]. The tritium-beam particle flux must be $I_{bT} = n_T/\tau_p$, or about 3 times the flux of the reacting $D^o$ beams. If the power of the fueling beams is not to exceed that of the reacting beams, then the voltage of the fueling beams can be up to one-third of that of the reacting beams. Therefore a considerable degree of penetration is assured, and the proportion

of D in the bulk plasma can probably be kept as small as 25%. An obvious disadvantage, however, is that the Q-value of the whole system is reduced by a factor of about two (if $W_{oD} \sim 3W_{oT}$). The finite pressure of the fueling beams may demand a significant reduction in $n_e$, so that $P_f$ is reduced by a factor of 1.2 to 1.4. A further disadvantage is that a significant fraction of the $T^o$ neutrals are trapped by charge exchange (because of their lower energy), thereby introducing an appreciable neutral population into the plasma.

2.2.5 50:50 D-T bulk plasma with D and T beams. If none of the above methods can be implemented, or if their drawbacks are intolerable, the most straightforward procedure is to treat deuterons and tritons in an identical fashion: One maintains a 50:50 D-T bulk plasma by injecting D and T neutral beams of equal velocity; fueling is carried out both by injected ions, and by plasma recycling. A shielding-unload divertor [15] is required for pumping, and to control the buildup of plasma density over long pulses, as well as to alleviate ion bombardment of the vacuum wall. While Q and $P_f$ are lower than in the ideal D→T method, the advantages of the present technique are that proper fueling is provided automatically, the power output is well-defined and constant during the pulse (in the absence of impurity buildup), and the fractional burn-up of tritium is relatively large. The length of the power pulse is limited fundamentally by the flux swing in the transformer core and could be many tens of seconds for a device of 1-m plasma radius. It is this mode of operation that we feel is most practical.

## 2.3 FURTHER CHARACTERISTICS OF 50:50 D-T OPERATION

We make two important specifications. First, we take $W_{oT} = 1.5\ W_{oD}$, so that the $D^o$ and $T^o$ beams have the same velocity, and therefore the same efficiency of production and penetration into the plasma. Second, we specify that both $D^o$ and $T^o$ beams be injected at a number of angles $\theta$ with respect to the magnetic axis - from $\theta = 0^o$ to nearly $90^o$ - for several reasons: (1) In steady-state, the velocity distribution is monotonically decreasing and nearly isotropic, and therefore is absolutely stable to velocity-space instabilities [1,17]. (2) If the thermal $D^+$ and $T^+$ have the same lifetimes, as seems likely, then the deuteron and triton particle injection rates must be the same. The injected triton scalar momentum is then 1.5 times larger, but multi-angle injection eliminates the possibility of a buildup in plasma momentum. (3) Overall penetration of the neutral beams is not as affected by a large impurity content in the plasma [18], compared with the case of purely tangentially injected beams. It is also more convenient to install beam ducts through the blanket and coil assemblies for oblique or perpendicular injection.

For plasmas of the size envisioned here ($I_p \gtrsim 1.5$ MA), loss cones in velocity space are relatively insignificant. However, ripples in the toroidal magnetic field must be minimized to avoid loss of mirror-trapped energetic ions. While tangential injection of oppositely directed T and D beams would maximize head-on nuclear collisions [8-10], such collisions are not particularly advantageous for the range of injection voltages ($\gtrsim$ 100 keV) required for penetration of the large plasmas to which the present work applies.

In the rest of this paper, we discuss the performance of steady-state 50:50 D-T plasmas in which $n_{hot}/n_e$ is in the range 0.01 to 0.3, and fusion reactions among superthermal ions are taken into account.

## 3. CALCULATIONAL MODEL

### 3.1 ENERGETIC-ION VELOCITY DISTRIBUTION

In the following, the subscript 1 refers to thermal ions at temperature $T_i$, while the subscript 2 refers to superthermal (hot) ions formed by neutral injection. Energetic ions whose energy falls below $2T_i$ are assumed to be absorbed by the thermal-ion distribution. In this work, we take $T_i = T_e$, a condition that is expected to hold rather well in a practical device for a number of reasons: Over most of the parameter range of interest, the energetic ions share their energy roughly equally between thermal ions and electrons; the equilibration time between thermal ions and electrons is comparable to $\tau_E$; a large proportion of the thermal-ion population, viz., a fraction $(n_2/n_1)(\tau_p/\tau_s)$, is formed directly from decelerated energetic ions. The thermal-ion population is taken as Maxwellian:

$$f_1(v) = n_1 \left(\frac{M_1}{2\pi T_i}\right)^{3/2} \exp\left[-\frac{M_1 v^2}{2T_i}\right] \qquad (3)$$

The steady-state velocity distribution, $f_2(\vec{v})$, of the energetic ions is calculated using the following model:

(1) Multi-angle injection at velocity $v_o$, so that $f_2(\vec{v})$ is isotropic.

(2) Particle sink at $v = v_m$, so that $f_2(v) = 0$, $v < v_m$.

(3) $v_e >> v_o >> v_i$, where $v_e$ and $v_i$ are the average thermal velocities of electrons and bulk ions.

(4) Ions with $v > v_m$ are perfectly confined.

(5) No Coulomb interaction among energetic ions.

(6) Energy diffusion during slowing-down is taken into account only in formation of the fast-ion tail above the injection velocity, $v_o$.

(7) The toroidal electric field is insignificant.

With these assumptions, the Fokker-Planck equation at $v \leq v_o$ becomes simply

$$f_2(v) v^2 \frac{dv}{dt} = \text{constant} \tag{4}$$

where dv/dt is the Coulomb deceleration of an energetic ion at velocity v. The solution to Eq. (4) is

$$f_2(v) = C_1 n_2 (v^3 + v_c^3)^{-1}, \quad v_m \leq v \leq v_o \tag{5a}$$

The tail at $v > v_o$ is produced by energy transfer from fast particles (electrons and ions) of the thermal plasma. If $T_i = T_e$, this tail is Maxwellian-like at temperature $T_e$:

$$f_2(v) = C_1 n_2 (v_o^3 + v_c^3)^{-1} \exp\left[ - \frac{M_2 (v^2 - v_o^2)}{2T_e} \right], \quad v > v_o \tag{5b}$$

The normalization constant, $C_1$, is given by

$$C_1 = \frac{1}{4\pi}\left\{\frac{1}{3}\ln\left(\frac{v_o^3 + v_c^3}{v_m^3 + v_c^3}\right)\right.$$

$$\left. + \frac{1}{v_o^3 + v_c^3}\frac{T_e}{M_2}\left[v_o + \exp\left(\frac{1}{2}\frac{M_2 v_o^2}{T_e}\right)\sqrt{\frac{\pi T_e}{2M_2}}\,\mathrm{erfc}\left(\sqrt{\frac{M_2}{2T_e}}\,v_o\right)\right]\right\}^{-1} \tag{5c}$$

In Equation (5), $v_c$ is the velocity at which the Coulomb drag forces exerted by the electrons and bulk-plasma ions are equal:

$$v_c = 5.44\left(\frac{T_e A_2}{M_2}\right)^{1/2}\left[\frac{1}{n_e}\frac{1}{\ln\Lambda_e}\sum_i \frac{n_i Z_i^2 \ln\Lambda_i}{A_i}\right]^{1/3} \tag{6}$$

Here $T_e$ is in keV, $A_i$ denotes atomic weight, and the summation is over the ion species of the bulk plasma. The Coulomb logarithms are calculated as in [11]. Even when $f_2(\vec{v})$ is not isotropic, Eqs. 5 describe the steady-state <u>scalar</u> velocity distribution, found by integrating $f_2(\vec{v})$ over all angles [1,17].

Figure 2 shows $f_1(v)$ and $f_2(v)$ for a number of values of $T_e = T_i$ and $n_2/n_e$, taking $v_m^2 = 4T_e/M_2$. In all cases, $f_2(v_m) \ll f_1(v_m)$. This velocity will be taken as the lower cutoff value for energetic ions, when calculating reactivities and slowing-down times.

The linear treatment becomes less valid with increasing $n_2/n_e$. For example, when $n_2/n_e \gtrsim 0.1$, the thermal-ion distribution function becomes somewhat distorted, the most notable change being a greatly extended tail due to strong interaction of background ions with energetic ions [19]. At the same time, Coulomb interaction among the energetic ions limits the validity of Eqs. (5) in describing $f_2(v)$. However, even when $n_2/n_e \sim 0.3$, the strength of the Coulomb interaction exerted by the energetic-ion population on a typical energetic ion is less than 20% of that exerted by the bulk ions, because of the much larger relative velocity, on the average, between energetic ions. Reference [20] shows that the main effect on $f_2(v)$ of energetic-ion interactions, at least when $n_2/n_e$ is not too large, is to broaden the tail at $v > v_o$ (which leads to an increase in Q).

Figure 2(a) compares $f_2(v)$ from Eqs. (5) with that calculated with a two-dimensional Fokker-Planck code [21], with isotropic injection and a sink at $v_m$. The two distributions are normalized at $v = v_c$, and are in excellent agreement for $v > 1.6\ v_m$. The fact that the peak value of the numerical Fokker-Planck solution occurs at $1.4\ v_m$ (rather than at $v_m$) is due to energy diffusion caused by interaction with the thermal ions ($v_i = 0.86\ v_m$). We find that the character of the numerical Fokker-Planck solution has very little variation for $.01 \lesssim n_2/n_e \lesssim 1/2$ [21], thus justifying the use of Eqs. (5) in this work, provided that $W_o$ and $T_i$ satisfy assumption (3).

A quantity of interest is

$$\Gamma = \frac{\text{energetic-ion pressure}}{\text{bulk-plasma pressure}} = \frac{\int_{v_m}^{\infty} f_2(v) \frac{1}{3} M_2 v^2 4\pi v^2 dv}{(n_e + n_1) T_e} \qquad (7)$$

For ideal D→T systems, $P_f$ is maximum when $\Gamma$ is in the range 0.70 to 0.96 [3], but this need no longer be the case for 50:50 D-T beam-driven plasmas. The range of parameters in this work includes $\Gamma > 1$. With isotropic $f_2(v)$, these systems are stable to velocity-space modes, provided that $v_o$ is less than the Alfven velocity [17].

## 3.2 FUSION ALPHA PARTICLES

Beam-driven tokamak plasmas of practical interest will have plasma current $I_p$ = 1.5 to 8 MA, and aspect ratio A = 3.5 to 6, so that at least 50% of the alpha particles resulting from fusion will be confined in the plasma [22]. For plasma conditions of interest here, $Q < 2$ (cf. Section 5). Then the pressure of the confined alphas is $p_\alpha \lesssim 0.2 Q p_{hot} \lesssim 0.25\ p_{total}$, if $\Gamma \lesssim 2$. In calculating neutron source characteristics in Section 7, we specify that $\beta_p \leq 2/3$ A, where $\beta_p$ is the total poloidal beta of the bulk plasma plus energetic ions. Therefore a 25% increase in pressure due to an alpha-particle population can be accommodated, without violating the MHD limit of $\beta_p$ = A.

For a given $n_e \tau_E$ and injection power, alpha heating will raise $T_e$ by up to 40% (for Q ~ 2), resulting in a further increase in Q. However, we find it more convenient to <u>specify</u> $T_e$, so that alpha heating is reflected by a lower requirement on $n_e \tau_E$, and need not be included directly when calculating fusion power densities.

We assume that thermalized alpha particles are removed by the magnetic divertor, so that there is no significant buildup of alphas during a power pulse. Therefore, by specifying $T_e$ and that $\beta_p \lesssim 2/3\ A$ (without alphas), we can ignore the alpha population in calculating Q and $P_f$. But calculations of the corresponding $n_e\tau_E$ must take alpha heating into account.

## 3.3 PLASMA PROFILES

In this work, a zero-dimensional spatial model is used in calculating Q and $P_f$. The average plasma pressure $\bar{p}$ allowed in a tokamak does not depend on the radial profiles of $n_e$ and $T_e$, but only on the toroidal field, $B_t$, the plasma aspect ratio, A, and the rotational transform at the limiter, q. To obtain the largest possible $\bar{p}$ in a given device, q should be as small as permitted by stable operation, and small q is facilitated by a flat $T_e(r)$. In practice, $n_e(r)$ may naturally have a rather flat (such as cubic) radial dependence, which can be regulated by the divertor [15]; while $T_e(r)$ can be controlled by adjusting the neutral beam deposition profiles. Specification of multi-angle injection allows one to control $T_e(r)$ by using different $W_o$ for beams injected at different angles $\theta$ to the magnetic axis. (Generally, the smaller $\theta$, the larger is $W_o$.)

If $Z_{eff}$ builds up during the power pulse, adequate penetration can be maintained by increasing the voltage of obliquely injected beams. At the same time, the current of the tangentially injected beams is decreased, in order that the total injected power be constant. The reactivities, Q-values, and burn-ups

presented in later sections are given as a function of $W_o$, so that average values for a particular system are readily calculated.

The results in this paper, except for those of Section 7, apply to all toroidal reactors where the bulk-plasma temperature is maintained solely by power deposition from energetic ions. The calculations in Section 7 apply specifically to tokamaks, but are easily generalized to other toroidal devices. It should be noted that in beam-driven tokamaks with $\bar{T}_e \gtrsim 3$ keV, $a_p \gtrsim 50$ cm, and $n_e\tau_E \lesssim 3 \times 10^{13}$ cm$^{-3}$s, ohmic power dissipation is negligible, even for $Z_{eff} >> 1$ [5].

## 4. FUSION REACTIVITIES

### 4.1 CALCULATION OF $\langle\sigma v\rangle$

Extending the notation of Section 3, subscripts 1 and 1' refer to thermal deuterons and tritons, respectively, while subscripts 2 and 2' refer to superthermal deuterons and tritons, respectively. The reactivity of two D and T components is

$$\langle\sigma v\rangle_{ij} = \frac{1}{n_i n_j}\iint f_i(v_i) f_j(v_j)\sigma(|\vec{v}_i - \vec{v}_j|)|\vec{v}_i - \vec{v}_j| d^3v_i d^3v_j \quad (8)$$

There are four possible combinations of (i,j):

$\langle\sigma v\rangle_{11'}$ denotes thermonuclear reactions,

$\langle\sigma v\rangle_{22'}$ denotes reactions among superthermal ions,

$\langle\sigma v\rangle_{1'2}$ denotes D→T (beam-target) reactions,

$\langle\sigma v\rangle_{12'}$ denotes T→D (beam-target) reactions.

$\langle\sigma v\rangle_{11'}$ can be reduced to a single integral by standard techniques, while $\langle\sigma v\rangle_{22'}$ requires the evaluation of a triple

integral, which is performed numerically using 32-point Gaussian-quadrature techniques. The beam-target reactivities require the numerical evaluation of double integrals.

Figures 3 and 4 show fusion reactivities calculated using $f_1(v)$ and $f_2(v)$ of Section 3.1, with $n_1 = n_{1'} = 0.45\ n_e$, so that $n_{hot}/n_e = 0.1\ n_e$. (The reactivities depend on this ratio through $v_c$.) The fusion cross sections are taken from Duane [23]. As expected, the D→TD and T→DT reactivities (Fig. 3) are nearly the same, for $W_{oT} \approx 1.5\ W_{oD}$. For $W_{oD} \gtrsim 150$ keV, the reactivities are relatively independent of $T_e$. (The chief effect of increasing $T_e$ is an increase in the cutoff velocity, $v_m$. Note that lowering the cutoff energy to $1.5\ T_e$ would actually reduce $\langle\sigma v\rangle_{1'2}$ and $\langle\sigma v\rangle_{12'}$, because the additional lower-energy ions have very small fusion probabilities.) The beam-target reactivities are typically more than an order of magnitude larger than the reactivity of the thermal plasma.

The hot-ion reactivities (Fig. 4) tend to be slightly smaller than the beam-target values, when $W_{oD} \gtrsim 150$ keV, but are slightly larger for $W_{oD} \lesssim 100$ keV. At small $T_e$, $\langle\sigma v\rangle_{22'}$ is rather close to that of a Maxwellian with $3/2\ T_i \approx \bar{W}$, where $\bar{W}$ is the average hot-ion energy (typically $\approx 0.5\ W_o$). The largest reactivity at low $T_e$ occurs for $W_{oD} \approx 150$ keV, for which $\bar{W} \approx 80$ keV. For parameters of greatest interest in reactor design, the values of $\langle\sigma v\rangle_{22'}$ fall in a very narrow range, viz. 0.8 to $0.95 \times 10^{-16}$ $cm^3/s$.

These reactivities are employed in the following sections to calculate neutron source characteristics.

## 4.2 RELATIVE NEUTRON SOURCE STRENGTHS

This section compares the neutron production rates per unit volume from the three types of reactions. The reaction-rate densities are

$R_{11'} = n_1 n_{1'} \langle \sigma v \rangle_{11'}$ (thermonuclear neutrons)

$R_{22'} = n_2 n_{2'} \langle \sigma v \rangle_{22'}$ (superthermal neutrons)

$R_{12'} = n_1 n_{2'} \langle \sigma v \rangle_{12'}$ (beam-target T→D neutrons)

$R_{1'2} = n_{1'} n_2 \langle \sigma v \rangle_{1'2}$ (beam-target D→T neutrons)

We prescribe $n_1 = n_{1'}$, so that the $D^o$ and $T^o$ particle injection rates must be equal. Since the background plasma is 50:50 D-T, and the $D^o$ and $T^o$ injected beams have the same velocity, then $\tau_{sT} = 3/2\ (1 + \varepsilon)\tau_{sD}$, where $\varepsilon(T_e) \lesssim 0.05$ takes into account that $v_m$ for $T^+$ is smaller than $v_m$ for $D^+$. Therefore, $n_{2'} = 3/2\ (1 + \varepsilon) n_2$ and charge neutrality demands that

$$n_e = 2n_1 + (5/2 + 3/2\varepsilon) n_2 \tag{9}$$

The relative reaction-rate densities are

$$\frac{R_{11'}}{R_{12'} + R_{1'2}} = \frac{\langle \sigma v \rangle_{11'}}{\langle \sigma v \rangle_{1'2} + 3/2(1 + \varepsilon)\langle \sigma v \rangle_{12'}} \left( \frac{n_1}{n_2} \right) \tag{10}$$

$$\frac{R_{22'}}{R_{12'} + R_{1'2}} = \frac{\langle \sigma v \rangle_{22'}}{\langle \sigma v \rangle_{12'} + \dfrac{\langle \sigma v \rangle_{1'2}}{3/2(1 + \varepsilon)}} \left( \frac{n_2}{n_1} \right) \tag{11}$$

These ratios are essentially independent of the absolute value of plasma density, which enters only through the weakly varying

Coulomb logarithms in $v_c$. Figure 5 shows the relative thermonuclear reaction rate (Eq. 10) as a function of $W_o$ and the relative superthermal-ion population, $n_{hot}/n_e = (n_2 + n_{2'})/n_e$. At $T_e = T_i = 4$ keV, thermonuclear reactions are negligible, unless the beam injection rate is minute (that is, $n_e\tau_E \gtrsim 10^{14}$ cm$^{-3}$s). At $T_e = T_i = 10$ keV, thermonuclear reactions contribute a significant fraction of the total fusion output. The relative contributions are nearly independent of injection energy.

Figure 6 compares the hot-ion and beam-target reaction rates (Eq. 11). The relative contribution of hot-ion reactions increases slightly faster than linearly with $n_{hot}/n_e$; it is nearly linearly proportional to the ratio $n_{hot}/2n_2$. The relative contribution of the hot-ion reactions is larger at smaller injection energies, which is evident from examination of Figs. 3 and 4. When $n_{hot}/n_e \sim 0.3$, hot-ion reactions increase the fusion output beyond the target-plasma level by 20 to 30%, while thermonuclear reactions provide up to 15% enhancement.

## 5. FUSION POWER GAIN

Although $Q_{D\rightarrow T}$ can be substantially greater than $Q_{T\rightarrow D}$ (cf. Figure 1), when the target plasma is 50:50 D-T, the Q-values for beam-target reactions of superthermal D and T ions injected at the same velocity are practically identical. As noted in Section 4.2, $\tau_{sT} = 3/2(1 + \varepsilon)\tau_{sD}$, where $\varepsilon << 1$, so that the 50% larger investment in triton energy is almost exactly compensated by the longer slowing-down time of the energetic tritons. The total fusion power gain $Q_f$, including all possible D-T reactions, is $Q_f = P_f/P_h$, where

$$P_f = E_f(R_{11'} + R_{22'} + R_{12'} + R_{1'2}) \tag{12}$$

with $E_f$ = 17.6 MeV, and

$$P_b = \sum_{i=2,2'} \int_{v_m}^{\infty} \left|\frac{dW}{dt}\right|_i f_i(v)\, 4\pi v^2 dv. \tag{13}$$

where dW/dt is the Coulomb energy loss rate. Alternatively, we may use

$$P_b = \frac{n_2}{\tau_{sD}} (W_{oD} - 2T_e) + \frac{n_{2'}}{\tau_{sT}} (W_{oT} - 2T_e) \tag{14}$$

where the $\tau_s$ are calculated by the slowing-down model in [11]. The two expressions for $P_b$ can give different values, since our calculation of $f_2(v)$ is strictly valid only when $v_i$ can be ignored, while the calculation of $\tau_s$ in [11] takes finite $v_i$ into account. With the assumptions in Section 3.1, we have

$$\left(\frac{dW}{dt}\right)_i = -\frac{C_2}{v} \sum_{1,1'} \frac{n_j \ln\Lambda_j}{A_j} - C_3 \frac{n_e}{T_e^{3/2}} v^2 \quad , \tag{15}$$

where $C_2$ and $C_3$ are constants. (A similar expression was used for dv/dt in Eq. (4).) Substituting Eq. (15) in Eq. (13), $P_b$ can be evaluated analytically. We find that $P_b$-values from Eqs. (13) and (14) agree to within 5% when $W_o \gtrsim 12\ T_e$. (For this comparison only, the tail in $f_2(v)$ was omitted.) In calculating Q, we use

Eq. (13), since this expression is consistent with the calculation of reactivities in $P_f$. In this and the following sections, we restrict the injection energy to $W_o \gtrsim 100$ keV, in order that our expression for $f_2(v)$ have good accuracy at $T_e \gtrsim 10$ keV.

The Q-values depend on $n_2/n_e$, but again are essentially independent of the absolute value of $n_e$, which enters only through the weakly varying Coulomb logarithms. D-D and T-T reactions have not been included, but these would increase Q only by 1-2%.

The required energy confinement time of the bulk plasma, so that its temperature can be sustained by injected superthermal ions together with alphas resulting from fusion, is

$$n_e\tau_E = \frac{3/2\ T_e n_e(n_e + 2n_1)}{P_b(1 + 0.2Q)} \qquad (16)$$

Here we have assumed that all fusion alphas thermalize with the bulk plasma (cf. Section 3.2). Evidently, $n_e\tau_E$ is essentially independent of $n_e$. If $0.2Q \ll 1$, then $n_e\tau_E$ is proportional to $T_e$ and nearly inversely proportional to $n_2/n_e$.

Figures 7 and 8 show Q and $n_e\tau_E$ as a function of the relative superthermal-ion population. For prescribed values of $n_{hot}/n_e$ and $T_e = T_i$, there is a broad maximum in Q for $150 \lesssim W_{oD} \lesssim 300$ keV. At low $T_e$, the required $n_e\tau_E$ decreases significantly with $W_o$, since $W_o/\tau_s$ increases, but the opposite dependence on $W_o$ holds at large $T_e$, where bulk-ion drag is dominant.

Now consider the variation of Q with $n_{hot}/n_e$.

(1) $n_{hot}/n_e < 0.1$. The injected beam power becomes relatively small, and can be surpassed by the thermonuclear power output,

resulting in $Q>>1$ [2,3]. However, $n_e\tau_E$ must be rather large in this region ($\gtrsim 5 \times 10^{13}$ $cm^{-3}s$), in order that the plasma temperature can be maintained by the small superthermal-ion population. (At very large temperatures, thermonuclear reactions contribute substantially to Q even when $n_{hot}/n_e > 0.1$ (cf. Fig. 5b).)

(2) $n_{hot}/n_e \gtrsim 0.1$. In any beam-driven system, increasing $n_2/n_1$ enables the bulk plasma to retain the same temperature at a smaller $n_e\tau_E$. But for an ideal D→T or T→D system, Q significantly decreases for $n_{hot}/n_e \gtrsim 0.1$, because of the gradual decrease in target density. For $n_{hot}/n_e \sim 0.1$, the Q-values of the 50:50 D-T system are only 0.5 to 0.7 those of the ideal D→T case. But as $n_{hot}/n_e$ increases, the additional hot-ion reactions compensate for the decrease in target-plasma reactions; as shown in Figs. 3 and 4, the reactivities are nearly the same. Thus, Q remains practically constant, as $n_e\tau_E$ decreases well below $10^{13}$ $cm^{-3}s$. (The confinement time of the hot ions, however, is determined by $\tau_s$, which tends to increase with increasing $n_{hot}/n_e$, because of the decrease in bulk-ion drag.) Thus hot-ion reactions become the most important contributor to fusion power at very small $n_e\tau_E$, while thermonuclear reactions are dominant at very large $n_e\tau_E$. In the limit of $n_{hot}/n_e \to 1$, the 50:50 D-T system goes over to the energetic-ion-dominated plasmas such as the CIT [8-10], where for counterstreaming low-energy D and T beams, Q may rise above the ideal D→T value.

In pure D→T systems, considerations of maximum $P_f$, satisfactory Q, and ease of beam penetration lead to the choice of $T_e = T_i \approx 6$ keV as the desirable operating point [3]. In the present 50:50 D-T systems, where Q-values are somewhat lower,

$T_e = T_i \approx 8$ keV seems a more reasonable choice. At $n_{hot}/n_e \gtrsim 0.1$, $Q \approx 0.7$-1.0, which is satisfactory for test-reactor and hybrid reactor applications. The corresponding $n_e\tau_E$ are in the range 0.6 to $2\times10^{13}$ $cm^{-3}s$. In Section 7, the "standard" operating temperature is taken as 8 keV.

## 6. FRACTIONAL TRITIUM BURN-UP

A large fractional burn-up of tritium per pass (i.e., once-through the machine) is desirable, since a larger burn-up reduces the tritium inventory required per unit fusion power output, and also reduces the demands on the tritium processing system. The fraction of beam-injected tritons that burn up during deceleration is

$$F_{b2'} = \frac{\tau_{sT}}{n_{2'}} (R_{22'} + R_{12'}) \tag{17}$$

Figure 9 shows $F_{b2'}$ as a function of $W_o$, $T_e$, and $n_{hot}/n_e$. For a given $T_e$, $F_{b2'}$ is roughly proportional to $W_o$; this behavior is expected, since Q is only weakly sensitive to $W_o$ (cf. Section 5). The near-invariance with $n_{hot}/n_e$ reflects the similarity of target-plasma and hot-ion reactivities.

The fraction of decelerated tritons that burn up during their lifetime $\tau_p$ in the thermal plasma is

$$F_{b1'} = \frac{\tau_p}{n_{1'}} (R_{11'} + R_{1'2}) \tag{18}$$

For typical plasma densities and currents, the plasma parameters tend to fall into the trapped-electron regime, where theoretical estimates [24] indicate that the thermal conduction rate, $\tau_E^{-1}$, is about 3 times the particle diffusion rate, $\tau_p^{-1}$.

Figure 10 shows $F_{bl'}$ for $\tau_p = 3\tau_E$; there is very little dependence on $W_o$. While $F_{bl'}$ can be very large at high $T_i$, where thermonuclear reactions are important, for $T_i \lesssim 10$ keV and $n_{hot}/n_e \gtrsim 0.1$, $F_{bl'}$ is only 1/4 to 1/3 $F_{b2'}$. Keeping in mind that plasma recycling is necessary to help maintain the plasma density in the reacting region (see Section 7.5), a given triton is recycled N times, where

$$N = \frac{\tau_u}{\tau_p} \frac{n_{1'}}{n_{2'}} - 1 \tag{19}$$

If there is no injection of gas into the torus, so that the recycling rate is controlled solely by a shielding-unload divertor [15], the total fractional burn-up of tritons once-through the machine is

$$F_{bT} = F_{b2'} + (N + 1)F_{bl'} \tag{20}$$

If $\tau_p \sim 3\tau_E \sim 2\text{-}3\tau_s$, then N is typically 2 or 3, and $F_{bT} \sim 2F_{b2'}$. Then for $4 \lesssim T_e \lesssim 10$ keV, $F_{bT}$ is in the range 1 to 4%, the maximum values being obtained at the largest $W_o$. There is very little sensitivity to $n_{hot}/n_e$.

At this point, it is appropriate to consider the relative advantages of injection at very large $W_o$: (1) The fractional tritium burn-up increases significantly with $W_o$. (2) Less beam current is required for a given injection power, thereby alleviating the problem of transmission through the beam ducts [25]. (3) Beam penetration into the central plasma region is facilitated,

especially when $Z_{eff} >> 1$. Offsetting these advantages are (1) the necessity to employ negative-ion beams, for $W_o > 200$ keV, in order to retain efficiency; (2) a somewhat smaller Q; (3) the possibility of exciting Alfven instabilities [17]. In any event, the most important factor in determining $W_o$ is the size of the plasma required to produce a desired fusion power output, or a desired wall loading. These topics are covered in the following section.

## 7. NEUTRON PRODUCTION RATES AND MAXIMUM WALL LOADINGS

### 7.1 MAXIMUM PLASMA DENSITY

The fusion power output from a reactor plasma of given size is limited by the maximum allowed plasma density. This density in turn is limited by one of the following restraints:

(1) The maximum pressure allowed by MHD equilibrium.

(2) The requirement that the injected neutral beams penetrate to the core of the plasma.

The plasma pressure is given by

$$p = 2.49 \times 10^{13} \left(\frac{B_t S}{qA}\right)^2 \beta_p \qquad (21)$$

where $B_t$ is the axial field in kG, p is in keV/cm$^3$, and

$$S = \text{plasma circumference}/2\pi a_p \ . \qquad (22)$$

The maximum electron density is then

$$(n_e)_{Ml} = \frac{p_{max}}{T_e + 2T_e \frac{n_1}{n_e} + 2/3\ \bar{W}_2 n_2/n_e + 2/3\ \bar{W}_2, n_2,/n_e} \qquad (23)$$

where $\bar{W}_2$ and $\bar{W}_2$, are the mean energies of the superthermal $D^+$ and $T^+$ (in keV). In Eq. (21), we take $(\beta_p)_{max} = 2/3\ A$ (cf. Section 3.2). The minimum practical value of A is limited by the minimum thicknesses of the ohmic-heating transformer core, the toroidal-field coils, and the inner shield. In this section, we use A = 4.0; then the geometric layout of essential reactor components determines a minimum $a_p$ of 75 cm. For plasma radii up to 2 m, the aspect ratio can not be reduced significantly below 3.5-4.0, since a larger transformer core is required to establish the larger discharge currents. While present tokamaks exhibit maximum $\tau_E$ at $q \gtrsim 3$ [12], the plasmas of interest here need have only relatively modest $n_e\tau_E$ for their size. Furthermore, since $T_e(r)$ can be regulated by the very intense beam injection, the current profile should be sufficiently flat so that q = 2.5 is grossly MHD stable. We adopt this value of q in our calculations.

The maximum field at the toroidal field coils falls in the range 70 kG (NbTi) to 150 kG ($Nb_3Sn$). With a 1.0-m shield on the small-R side of the torus vacuum vessel, taking A = 4.0, and varying $R_o$ in the range 3 to 6 m, the corresponding fields on the magnetic axis lie in the range 25 to 70 kG.

Next consider the problem of beam penetration. Defining $\lambda_t$ as the neutral-beam trapping length for 1/e attenuation, then adequate penetration is attained for tangential injection when $\lambda_t/a_p \gtrsim 0.5$, while for perpendicular injection,

$\lambda_t/a_p$ as small as 0.25 is permissible [26]. While we specify oblique injection at a number of angles from tangential to perpendicular, we also use the condition $\lambda_t/a_p \geq 0.5$, in order to allow for the possibility of $Z_{eff} > 1$. (At large $Z_{eff}$, tangential injection is not required to insure a nearly isotropic $f_2(v)$. Employing oblique injection alone aids penetration, and enhanced pitch-angle scattering serves to isotropize the fast-ion velocities.) The effect of $Z_{eff}$ on penetration is considered specifically in [18,27].

As explained in Section 3.3, we assume uniform $n_e(r)$, $T_e(r)$. Then a second limitation on the electron density is

$$(n_e)_{M2} = \frac{2}{a_p} \frac{v_o}{\Sigma \langle \sigma v \rangle_I} \tag{24}$$

where $\Sigma \langle \sigma v \rangle_I$ is the sum of the rate coefficients for ionization by charge exchange, ion-impact ionization, and electron ionization [28]. (In calculating $\lambda_t$, we treat <u>all</u> plasma ions as stationary. Actually, when $n_2/n_e$ is large, an appreciable number of thermal ions are replaced by fast ions. On the average, the relative velocity between the injected neutral and the plasma ions is increased, so that ionization cross sections are reduced, and $\lambda_t$ is larger. Therefore, the present calculation gives us additional margin in the event that $Z_{eff} > 1$.)

In calculating neutron production rates, we use the minimum of $(n_e)_{M1}$ and $(n_e)_{M2}$. For a given plasma size, $(n_e)_{M2}$ is the limiting density for small $W_o$, while $(n_e)_{M1}$ is the limit for large $W_o$. Our range of injection energies extends to 400 keV for $D^o$ (600 keV for $T^o$). With positive-ion beam technology and the use

of direct conversion of unneutralized ions, injection efficiency can be as large as 40% for $W_o \approx 250$ keV [29], and efficiency increases at smaller $W_o$. Efficient beam injection at $W_o \gtrsim 250$ keV requires the difficult technology of negative-ion sources.

## 7.2 MAXIMUM NEUTRON PRODUCTION RATE

The total reaction rate per unit volume is

$$R_t = n_e^2 \left\{ \left( \frac{n_1}{n_e} \right)^2 \langle \sigma v \rangle_{11'} + \frac{n_2}{n_e} \frac{n_{2'}}{n_e} \langle \sigma v \rangle_{22'} \right. \\ \left. + \frac{n_1}{n_e} \frac{n_{2'}}{n_e} \langle \sigma v \rangle_{12'} + \frac{n_{1'}}{n_e} \frac{n_2}{n_e} \langle \sigma v \rangle_{1'2} \right\} \tag{25}$$

Given $n_2/n_e$, $T_e$, and $W_o$, the maximum value of $R_t$ is found by substituting Eq. (23) or (24) for $n_e$. In order to express areas and circumferences in terms of S, we take the elliptical cross section as illustrative. Then $S = (1 + b^2/a_p^2)^{1/2}/\sqrt{2}$, where b is the length of the vertical half-axis. The neutron production rate from a plasma of mid-plane radius $a_p$, with A = 4.0, is

$$P_n = R_t 8\pi^2 a_p^3 (2S^2 - 1)^{1/2} \tag{26}$$

Figure 11 shows the variation of $P_n$ with plasma radius and injection energy, at $B_t = 50$ kG and $S = 1.0$. For each $a_p$, there is an optimum $W_o$ for maximum $P_n$, which occurs when $(n_e)_{M1} = (n_e)_{M2}$. $(P_n)_{max}$ is in the range $2\times10^{19}$ to $2\times10^{20}$ $s^{-1}$, and increases roughly as $a_p^{2.4}$. For a given $a_p$, there is little variation in

$(P_n)_{max}$ with $n_{hot}/n_e$, but the optimal $W_o$ is reduced by increasing $n_{hot}/n_e$. This shift reflects the facts that the pressure-limiting density (Eq. 23) is attained at smaller $W_o$, when $n_{hot}/n_e$ is larger, and that hot-ion collisions are more important at smaller $W_o$ (Fig. 6).

Figure 12 shows the relation between Q and $P_{out}$, the total fusion power output, for plasmas of given radius. With constant $W_o$ and $n_{hot}/n_e$, there is a unique relation between $n_e\tau_E$ and Q, such as indicated in Fig. 7. In order to obtain the desired trade-off between Q and $P_{out}$, it is necessary to adjust $n_e\tau_E$ [3], which controls $T_e$ and therefore Q. The power output increases monotonically with $a_p$, as also found by Sheffield [27] for the ideal D→T case. At a given $a_p$, $P_{out}$ has a maximum in $n_e\tau_E$, and therefore in $T_e$. The dots denote $T_e$ = 8 keV, our "standard" operating temperature, which gives Q-values slightly less than unity, and output powers not far from the maximum attainable values. The maximum injected power, $P_{out}/Q$, tends to occur at very low $T_e$.

## 7.3 MAXIMUM NEUTRON WALL LOADING

For certain applications, such as materials testing or actinide burning [30], large neutron wall loading is a more important performance criterion than the total fusion power output. For plasmas and vacuum vessels of elliptical cross section, the neutron wall loading (in $W/cm^2$) is

$$\phi_w = 2.26\times10^{-12} R_t \pi a_p^2 (2S^2 - 1)^{1/2}/C_w \qquad (27)$$

where the wall circumference is

$$C_w = \pi\sqrt{2}(a_p + \Delta)\left[1 + \left(\frac{b + \Delta}{a_p + \Delta}\right)^2\right]^{1/2} \qquad (28)$$

Here $\Delta$ is the width of the plasma scrape-off channel, which we take as 20 cm.

Figure 13 shows the variation of $\phi_w$ with plasma radius and injection energy, for S = 1.0 and $B_t$ = 50 kG. Maximum $\phi_w$ varies roughly as $a_p^{1/2}$, as expected for circular plasmas in which the maximum fusion output varies as $a_p^{2.4}$ (Section 7.2), and A is constant. As $n_{hot}/n_e$ increases, the wall loading increases somewhat, but the principal effect is a shift in the optimal $W_o$ to lower values, as for $P_n$. Except at small $W_o$, it turns out that $\phi_w$ decreases with increasing $T_e$, but the trade-off in Q and $\phi_w$ (analogous to Fig. 12) indicates that temperatures around 8 keV are the most attractive.

Figures 12 and 13 indicate how reactor parameters can be chosen most appropriately for a given application. (1) For devices such as engineering test reactors [4], where maximum $\phi_w$ and minimum injection power are desirable (i.e., to maximize $\phi_w/P_b$), one should operate with $a_p \lesssim 1.0$ m, and employ $W_o$ in the range 125-200 keV. (2) When both maximum $\phi_w$ and maximum power output are required, as in certain hybrid reactors, one should operate at $a_p \gtrsim 1.5$ m. The optimal $W_o$ can be kept near 200 keV, by going to $n_{hot}/n_e \gtrsim 0.2$ (Fig. 13).

## 7.4 EFFECT OF MAGNETIC FIELD AND PLASMA ELONGATION

With circular plasmas of radius $\lesssim$ 2 m, and $B_t \lesssim$ 50 kG, the neutron wall loading in 50:50 D-T reactors is limited to at most 1 MW/m$^2$. We now investigate whether appreciably higher $\phi_w$ can be

attained by increasing $B_t$ and S, keeping A = 4.0. Our "standard" injection energy for $D^o$ is 200 keV (300 keV for $T^o$), since previous sections have indicated that this value is the most widely useful. Generally, the dependences of $P_{out}$ or $\phi_w$ on S and $B_t$ are formally similar, and it is commonly thought that one can be traded off against the other - that is, the technological difficulties of operating with very large $B_t$ can be traded off against the physical difficulties of maintaining stable plasmas at large S and low q.

Figure 14 shows the effect of increasing $B_t$ at S = 1.0. For each $a_p$, there is a minimum $B_t$, above which $n_e$ is fixed by the requirement of acceptable beam penetration (Eq. 24). The largest $\phi_w$ are now attained at the smallest $a_p$, where $n_e$ is pressure-limited through most of the practical range of $B_t$. For small $a_p$, $\phi_w \propto B_t^4$. Nevertheless, the maximum $\phi_w$ for circular plasmas is still limited to about 1 $MW/m^2$, although somewhat larger values can be obtained by reducing $T_e$ below 8 keV, or by employing larger injection energies when $a_p > 1.5$ m.

Figure 15 shows the effect of increasing the vertical elongation of the plasma, when $B_t$ = 50 kG. For each $a_p$, there is a minimum S above which $n_e$ is nearly fixed by the beam-penetration requirement. The wall loadings increase significantly with $n_{hot}/n_e$; when the hot-ion pressure is small, the plasma density is already near the penetration-limited value (Eq. 24) when S = 1. A wall loading as large as 2.5 $MW/m^2$ can be attained at $a_p$ = 75 cm, when $n_{hot}/n_e = 0.3$, and S = 1.75 ($b/a_p = 2.26$). For small $a_p$ and small S, $\phi_w$ increases nearly as $S^4$.

Another approach to calculating the variation of maximum wall loading with magnetic field and plasma elongation is the following.

The geometrical dimensions of the components on the small-major-radius side of the torus are fixed as follows: transformer core radius = 1.2 m, TF (toroidal field) coil thickness = 0.65 m, shield thickness = 1.0 m, $\Delta$ = 0.25 m. Then the inner edge of the plasma is located at R = 3.1 m. The maximum TF field, $B_M$, occurs at R = 1.85 m. For given values of $B_M$ and $b/a_p$, $\phi_w$ is maximum when $n_e$ is limited <u>both</u> by adequate neutral-beam penetration and by the plasma pressure limitation; that is, $(n_e)_{M1} = (n_e)_{M2}$, or

$$\frac{2}{a_p} = C_4 \frac{a_p[1 + (b/a_p)^2]B_M^2}{(3.1 + a_p)^3} \qquad (29)$$

where $C_4$ is a constant for given values of $W_o$, $T_e$ and $n_{hot}/n_e$. Equation (29) can be solved for $a_p$, and the corresponding $\phi_w$ calculated from Eq. (27). In the present approach to calculating $\phi_w$, the plasma aspect ratio may depend strongly on both $B_M$ and $b/a_p$. For $a_p << 3.1$ m ($A >> 1$), it is easily shown that $\phi_w$ is approximately proportional to $B_M$ and to $b/a_p$. In the same approximation, the required injection power is nearly proportional to $b/a_p$, and nearly independent of $B_M$.

Theoretical considerations indicate that the largest vertical elongation for which stable operation is possible at low q is $b/a_p \sim 2$ to 3 [12,31]; for an elliptic cross section, $b/a_p = 3$ corresponds to S = 2.2. (In practice, stability at low q will require a D-shaped, rectangular, or doublet cross section [12,31].) Figure 16 shows the variation of maximum $\phi_w$ with both $b/a_p$ and $B_M$, for $W_o$ = 200 keV and $T_e = T_i$ = 8 keV. At small $b/a_p$ and small $B_M$,

both $a_p$ and $I_p$ must be extremely large to satisfy Eq. (29); in Fig. 16, we include only regions where $I_p < 10$ MA. As expected, $\phi_w$ increases fairly linearly with both $b/a_p$ and $B_M$. (This behavior is to be contrasted with the $B^4S^4$ behavior when $n_e$ is below the penetration-limiting value, as in Figs. 14 and 15.) While there is a trade-off between large magnetic field (i.e., $Nb_3Sn$ coils) and plasma elongation, both are needed in order to attain the largest wall loadings.

Increasing the relative proportion of energetic ions results in a significant increase in $\phi_w$. For example, $\phi_w$ increases by approximately 60% when $n_{hot}/n_e$ is raised from 0.1 to 0.3. However, the total injected power must increase by an even larger factor, since the plasma volume turns out to be somewhat larger in the $n_{hot}/n_e = 0.3$ case, and the Q-value is slightly smaller (cf. Fig. 7). The operating conditions of Fig. 16(a) are most appropriate for maximizing $\phi_w/P_b$, while the conditions of Fig. 16(b) are most appropriate for maximizing both $\phi_w$ and $P_{out}$.

The procedure just described for maximizing $\phi_w$ evidently corresponds to operating at the "knees" of the curves in Figs. 14 and 15. An increase in $b/a_p$ or in $B_M$ results in an increase in the pressure-limited density, so that the plasma radius must be reduced to allow satisfactory penetration of the injected beams. Thus with increasing $b/a_p$ or $B_M$, we advance from the knee of one $a_p$ contour to the knee of a smaller-$a_p$ contour. (This description is only approximate, since the curves in Figs. 14 and 15 are calculated for constant aspect ratio.) In practice, high-power operation at very small $a_p$ would be extraordinarily difficult, because of the problems of neutral-beam access [25]: When using the

present method to optimize the plasma size for the largest neutron wall loading, the plasma volume always decreases, while $P_b$ must increase almost linearly with $b/a_p$, as shown in Fig. 16, although it can drop slightly with increasing $B_M$.

## 7.5 ROLE OF THE MAGNETIC DIVERTOR

For typical operating conditions such as $W_{oD}$ = 200 keV, $T_e$ = 8 keV, $n_{hot}/n_e$ = 0.20, we have $\tau_s/\tau_E$ = 2.0. If $\tau_p \approx 3\tau_E$ [12,24], the particle outflow from the plasma is $2n_1/\tau_p \approx 2.7n_{hot}/\tau_s$. Taking $P_b$ = 300 MW, the injection rate is $7.5\times10^{21}$ particles/s, while the outward flow rate is $2\times10^{22}$ particles/s. This particle outflux cannot be handled by cryopumping in ducts surrounding the torus, if the gas pressure in the beam ducts is to remain sufficiently low that neutral beam transmission is not impeded (i.e., $p \lesssim 3\times10^{-5}$ torr). Furthermore, under the above conditions, the injected beams supply approximately 35% of the particle outflow rate, so that if the plasma density is to be constant, 65% of the exiting ions must be recycled. On the average, an outgoing ion must be recycled 1.7 times (cf. Eq. 19).

The pumping requirement can be met if outflowing ions flow rapidly into a burial chamber. The functions of a magnetic divertor in the present context include: (1) regulation of the pumping and recycling of outflowing plasma ions, so that $n_e$ is maintained constant throughout the power pulse, while the gas pressure outside the discharge region is kept small; (2) removal of energy from the torus, thus alleviating bombardment of the wall; (3) shielding of the plasma from impurities sputtered from the wall.

These requirements can be met by a shielding-unload divertor with a wide scrape-off channel (~ 10 cm) that captures all ions crossing the separatrix, and which is particularly suited for quasi-stationary fueling [32]. The plasma ions flowing into the burial chamber do recombine, but the pressure in this chamber is maintained at an appropriate level, so that many neutrals are re-ionized. The result is a net slowing down of the plasma outflow, to an extent determined by the regulated pressure in the burial chamber. In order that 2/3 of the plasma, for example, be recycled, the pressure in the burial chamber must be of order $5\times10^{-5}$ torr.

There is no recycling of neutrals in the torus itself. Since the cold shield plasma of the scrape-off channel completely traps the exiting ions, there should be negligible gas buildup in the torus, or in the beam ducts [32]. The load on the cryopumps in the beam ducts is then determined essentially by gas flowing from the ion sources and neutralizers. This type of divertor would also be effective in ionizing and trapping impurities sputtered from the wall [15].

## 8. CONCLUSIONS

The problems of plasma fueling and exhaust for high-duty-factor, constant-output performance of intensely beam-driven tokamak reactors may compel a 50:50 D-T mode of operation, with the bulk-plasma temperature ($T_e \approx T_i$) maintained by injection of both D and T neutral beams of equal current and velocity. A shielding-unload divertor is required to pump the plasma outflux, and to control the recycling of plasma ions.

When both D and T are neutral-beam injected with comparable intensities, fusion reactions between energetic ions can contribute significantly to the total fusion power output, $P_{out}$. Neutron source characteristics are determined most conveniently by means of fusion reactivities calculated separately for energetic-ion reactions, target-plasma reactions, and thermonuclear reactions. For $n_{hot}/n_e \lesssim 0.3$, and $W_o \geq 12\ T_e$, these reactivities can be calculated sufficiently accurately using energetic-ion distribution functions determined from the Fokker-Planck equation without energy diffusion (but including an energetic tail above the injection velocity). Multi-angle injection is specified, so that the hot ions have isotropic velocity distributions. For conditions where $Q \sim 1$, beam-target reactions are dominant, although energetic-ion reactions make a substantial contribution to $P_{out}$ when $n_{hot}/n_e \gtrsim 0.2$. With increasing $n_{hot}/n_e$, a given Q-value $\lesssim 1$ can be maintained with $n\tau_E$-values substantially below $10^{13}$ $cm^{-3}s$.

When tritium is injected via energetic neutral beams (rather than by pellets or gas), the fractional burn-up of tritium per

pass is maximized. For $T_e$ = 6 to 10 keV, and $W_o$ = 200 keV, the burnup rate once-through the reactor is 2 to 3%.

The variation of $P_{out}$ and neutron wall loadings with several plasma parameters has been determined, when the plasma density is limited either by the requirement of adequate neutral-beam penetration, or by the plasma pressure limitation. Given $W_o$, radius, and $n_{hot}/n_e$, $P_{out}$ has a maximum in $T_e$ (which is determined by $n\tau_E$), and therefore in Q. An operating temperature suitable for many applications is $T_e$ = 8 keV, which results in Q-values slightly less than unity, but with $P_{out}$ near the maximum possible value.

For circular cross-section plasmas, the 14-MeV neutron wall loading, $\phi_w$, is limited to little more than 1 MW/m$^2$ at Q ~ 1, even at the largest practical magnetic field strengths. Larger wall loadings are possible by vertical elongation of the plasma, when $n_{hot}/n_e \gtrsim 0.1$. Maximum $\phi_w$ is obtained when the plasma density is limited both by the neutral-beam penetration, and by the MHD limit on the total pressure. If the geometrical dimensions of the inner tokamak components are fixed, and the plasma radius adjusted to satisfy the above condition, then $\phi_w$ increases approximately proportional to both magnetic field and vertical elongation, b/a. With $W_o$ = 200 keV and $T_e$ = 8 keV, $\phi_w \approx 4$ MW/m$^2$ is attainable with maximum field at the TF coils of 140 kG and b/a = 3.

In 50:50 D-T operation, utilizing both D and T injection with the same intensity and velocity, the use of relatively large values of $n_{hot}/n_e$ may have several advantages: The largest $\phi_w$ are obtainable for given-sized devices (but at the price of larger injection power); $n_e\tau_E$ is smallest; and for a given power output or $\phi_w$, the neutral-beam voltage can be minimized.

REFERENCES

[1] BERK, H. L., et al., in Plasma Physics and Controlled Nuclear Fusion Research (Proc. 5th Int. Conf., Tokyo, 1974), paper CN-33/G2-3 (to be published).

[2] FURTH, H. P., JASSBY, D. L., Phys. Rev. Lett. 32 (1974) 1176; see also CORDEY, J. G., CORE, W. G. F., SHEFFIELD, J., Nucl. Fusion 15 (1975) 755; CONN, R. W., KESNER, J., Nucl. Fusion 15 (1975) 775; CUEST, G., MCALEES, D. G., Nucl. Fusion 14 (1974) 703; MILEY, G. H., TOWNER, H. H., Proc. Conf. on Nuclear Cross Sections and Technology (Washington, 1975).

[3] JASSBY, D. L., Nucl. Fusion 15 (1975) 453.

[4] CONN, R. W., JASSBY, D. L., Univ. Wisconsin Rep. FDM-119 (1975), to be published.

[5] JASSBY, D. L., Princeton Plasma Physics Lab. Rep. MATT-1115 (1975).

[6] GOLOVIN, I. N., et al., Kurchatov Institute of Atomic Energy Reports (1974).

[7] LIDSKY, L. M., Nucl. Fusion 15 (1975) 151; BOGART, S. L., ed., Proc. DCTR Fusion-Fission Energy Systems Review Meeting (Washington, 1974), U.S.E.R.D.A. Report ERDA-4 (1975).

[8] JASSBY, D. L., KULSRUD, R. M., SUN, Y. C., Proc. Seventh European Conf. on Controlled Fusion and Plasma Physics (Lausanne, 1975) I, 25.

[9] JASSBY, D. L., Princeton Plasma Physics Lab. Rep. MATT-1145 (1975).

[10] CORDEY, J. G., CORE, W. G. F., Nucl. Fusion 15 (1975) 710.

[11] SIVUKHIN, D. V., in Reviews of Plasma Physics (Consultants Bureau, New York, 1966) vol. 4, 93-128.

[12] FURTH, H. P., Nucl. Fusion 15 (1975) 487.

[13] GRALNICK, S., Nucl. Fusion 13 (1973) 703.

[14] BOTTIGLIONI, F., COUTANT, J., FOIS, M., Nucl. Fusion 14 (1974) 365.

[15] MEADE, D. M., et al., in Plasma Physics and Controlled Nuclear Fusion Research (Proc. 5th Int. Conf., Tokyo, 1974), paper CN-33/A15-4 (to be published).

[16] MILLS, R. G., in Proc. First Int. School of Fusion Reactor Technology (Erice, 1972) EUR 4999, p. 325.

[17] BERK, H. L., et al., Nucl. Fusion 15 (1975) 819.

[18] GIRARD, J. P., MARTY, D., MORIETTE, P., in Plasma Physics and Controlled Nuclear Fusion Research (Proc. 5th Int. Conf., Tokyo, 1974), paper CN-33/A17-2 (to be published).

[19] CORDEY, J. G., in Plasma Physics and Controlled Nuclear Fusion Research (Proc. 5th Int. Conf., Tokyo, 1974), paper CN-33/A16-1 (to be published).

[20] CORDEY, J. G., CORE, W. G. F., Phys. Fluids 17 (1974) 1626.

[21] SUN, Y. C., unpublished.

[22] MCALEES, D. G., Oak Ridge National Lab. Rep. ORNL-TM-4661 (1974).

[23] DUANE, B. H., Battelle Pacific Northwest Lab. Rep. BNWL-1685 (1972).

[24] ADAM, J. C., TANG, W. M., Princeton Plasma Physics Lab. Rep. MATT-1156 (1975).

[25] RIVIERE, A. C., SHEFFIELD, J., Nucl. Fusion 15 (1975) 944.

[26] ROME, J. A., CALLEN, J. D., CLARKE, J. F., Nucl. Fusion 14 (1974) 141.

[27] SHEFFIELD, J., Proc. Seventh European Conf. on Controlled Fusion and Plasma Physics (Lausanne, 1975) I, 21.

[28] RIVIERE, A. C., Nucl. Fusion 11 (1971) 363.

[29] HOVINGH, J., MOIR, R. W., Nucl. Fusion 14 (1974) 629; see also FINK, J. H., Lawrence Livermore Lab. Rep. UCRL-51650 (1974).

[30] ROSE, R. P., et al., Westinghouse Electric Corp. Reports WFPS-TME-003, 024 (1975).

[31] SHAFRANOV, V. D., YURCHENKO, E. I., Nucl. Fusion 8 (1968) 329; see also OKABAYASHI, M., SHEFFIELD, G., Nucl. Fusion 14 (1974) 263.

[32] MEADE, D. M., private communication.

## SYMBOLS

| | |
|---|---|
| $a_p$ | plasma minor radius |
| $A$ | aspect ratio, $R_o/a_p$ |
| $b$ | half-height of elliptic plasma |
| $B_t$ | toroidal field on magnetic axis |
| $B_M$ | maximum toroidal field (at coil) |
| $B_p$ | poloidal field |
| $C_1, C_2, C_3, C_4$ | constants |
| $C_w$ | circumference of vacuum wall |
| $E_f$ | yield of D-T reaction (17.6 MeV) |
| $f_1, f_2$ | velocity distribution of thermal ions, energetic ions |
| $F_b$ | fractional burn-up of tritium per pass |
| $I_b$ | injection rate |
| $I_p$ | plasma current |
| $M_1, M_2$ | mass of thermal ion, energetic ion |
| $n_e$ | electron density |
| $(n_e)_{M1}$ | maximum density permitted by pressure limitation |
| $(n_e)_{M2}$ | maximum density permitted by neutral-beam penetration |
| $n_1, n_1'$ | density of thermal deuterons, tritons |
| $n_2, n_2'$ | density of energetic deuterons, tritons |
| $n_{hot}$ | $n_2 + n_2'$ |
| $N$ | number of times a triton is recycled |
| $p$ | plasma pressure |
| $P_b$ | injection power density |
| $P_f$ | fusion power density |
| $P_n$ | total neutron production rate |
| $P_{out}$ | total fusion power output |
| $q$ | safety factor at the limiter |
| $Q$ | fusion power multiplication factor |
| $R_o$ | major radius (magnetic axis) |
| $R_{ij}$ | reaction-rate density for reactions among (i,j) components |
| $R_t$ | total reaction-rate density |
| $S$ | plasma circumference/$2\pi a_p$ |
| $T_e$ | electron temperature |

| | |
|---|---|
| $T_i$ | ion temperature |
| $v_c$ | velocity at which electron drag = bulk-ion drag |
| $v_e$ | electron thermal velocity |
| $v_i$ | bulk-ion thermal velocity |
| $v_m$ | "sink" velocity for energetic ions |
| $v_o$ | injection velocity |
| $W_o$ | injection energy |
| $\bar{W}_2, \bar{W}_2'$ | mean energy of superthermal deuterons, tritons |
| $Z_{eff}$ | effective ionic charge |
| $\beta_p$ | plasma beta in the poloidal magnetic field |
| $\Gamma$ | ratio of energetic-ion energy density to bulk-plasma energy density |
| $\lambda_t$ | mean-free-path for trapping of injected neutral |
| $\langle\sigma v\rangle_{ij}$ | fusion reactivity for reactions among (i,j) components |
| $\tau_E$ | energy confinement time |
| $\tau_p$ | particle confinement time |
| $\tau_s$ | slowing-down time of energetic ions |
| $\phi_w$ | neutron wall loading |

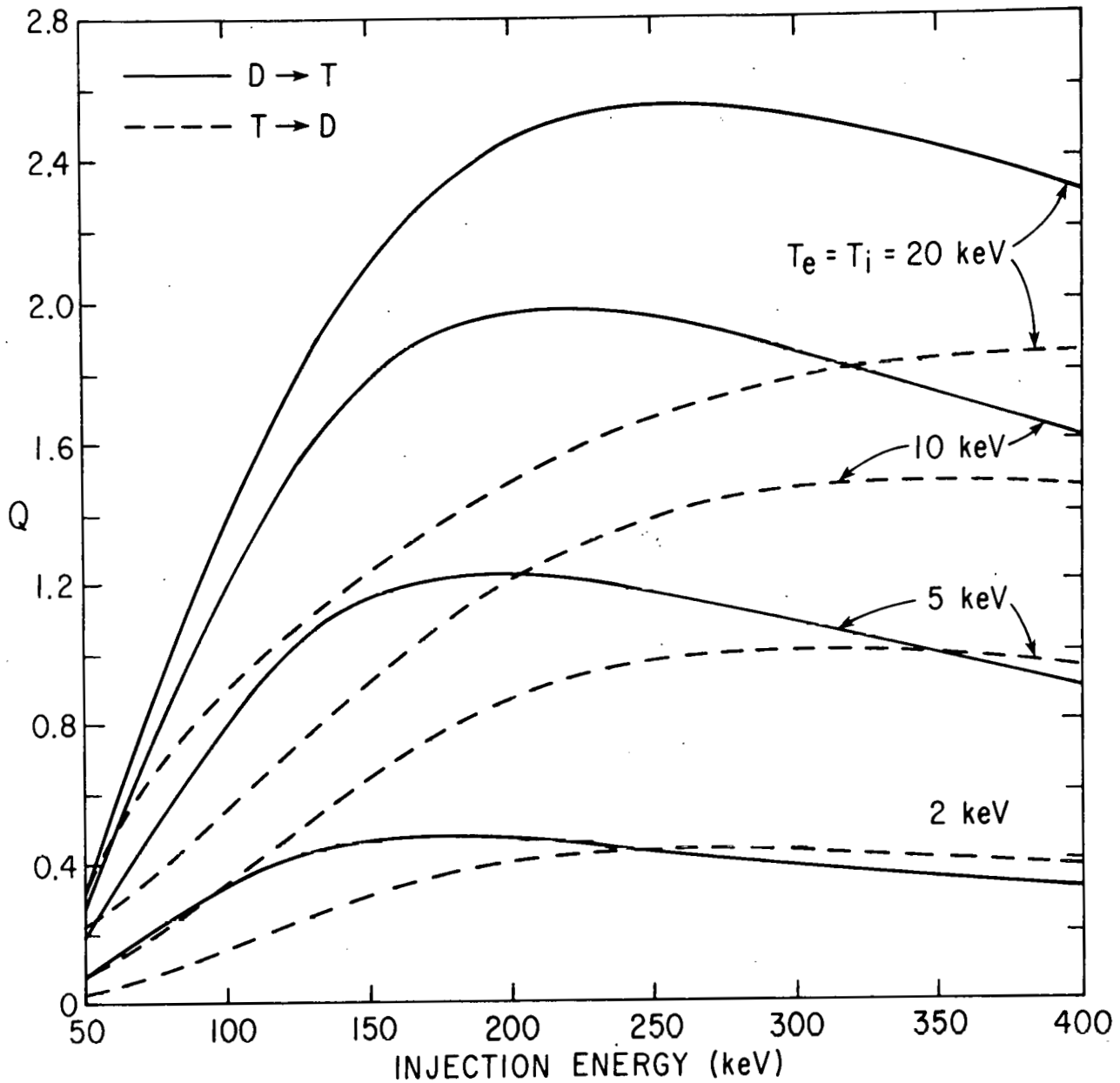


753987

Fig. 1. Fusion power multiplication for an energetic deuteron injected into a tritium background plasma (D→T), or an energetic triton injected into a deuterium plasma (T→D), taking 17.6 MeV per reaction. Target ions are Maxwellian with $T_i = T_e$. Coulomb logarithms are calculated at $n_e = 10^{14}$ cm$^{-3}$.

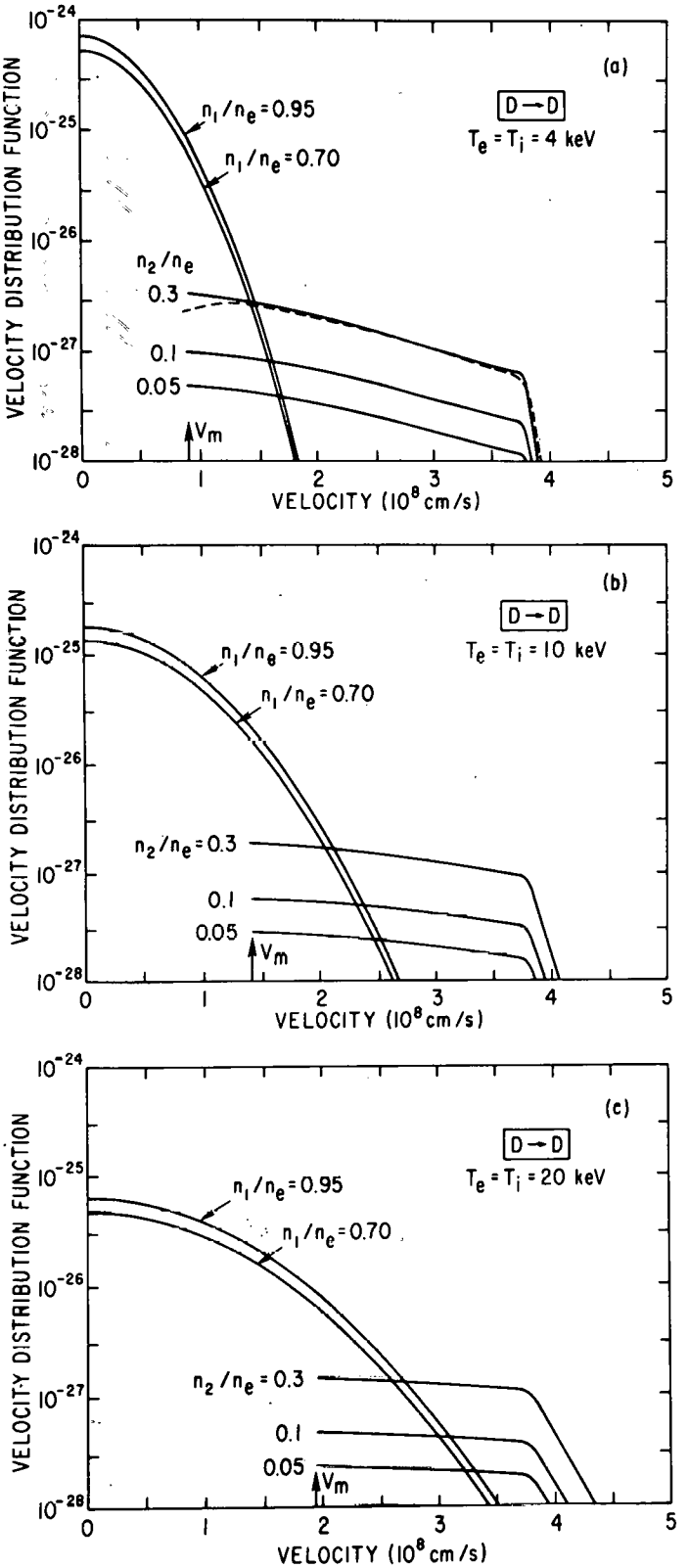


756048

Fig. 2. Steady-state velocity distributions for energetic deuterons of density $n_2$ injected at 150 keV ($3.8\times10^8$ cm/s) into a deuterium background plasma with Maxwellian ions of density $n_1$ and temperature $T_i = T_e$. $v_m$ is the deuteron velocity at $W = 2T_e$. The dashed line in (a) is the result of a numerical Fokker-Planck calculation.

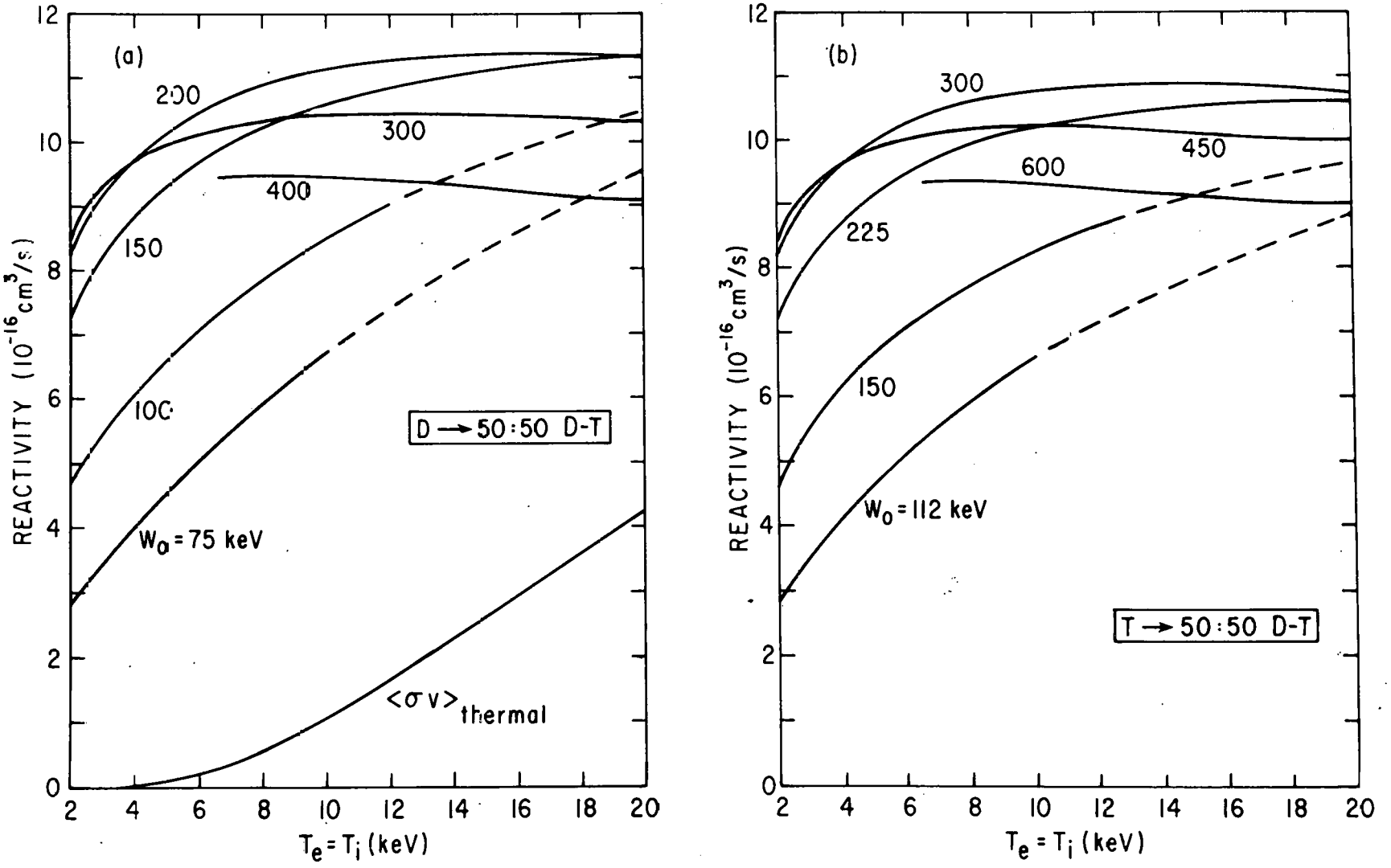


753989

Fig. 3. Fusion reactivities for target-plasma reactions of (a) deuterons and (b) tritons injected at energy $W_o$ into a 50:50 D-T plasma at temperature $T_e = T_i$. Isotropic, steady-state distribution of energetic ions. $\langle \sigma v \rangle_{thermal}$ is the reactivity of the target ions at temperature $T_i$.

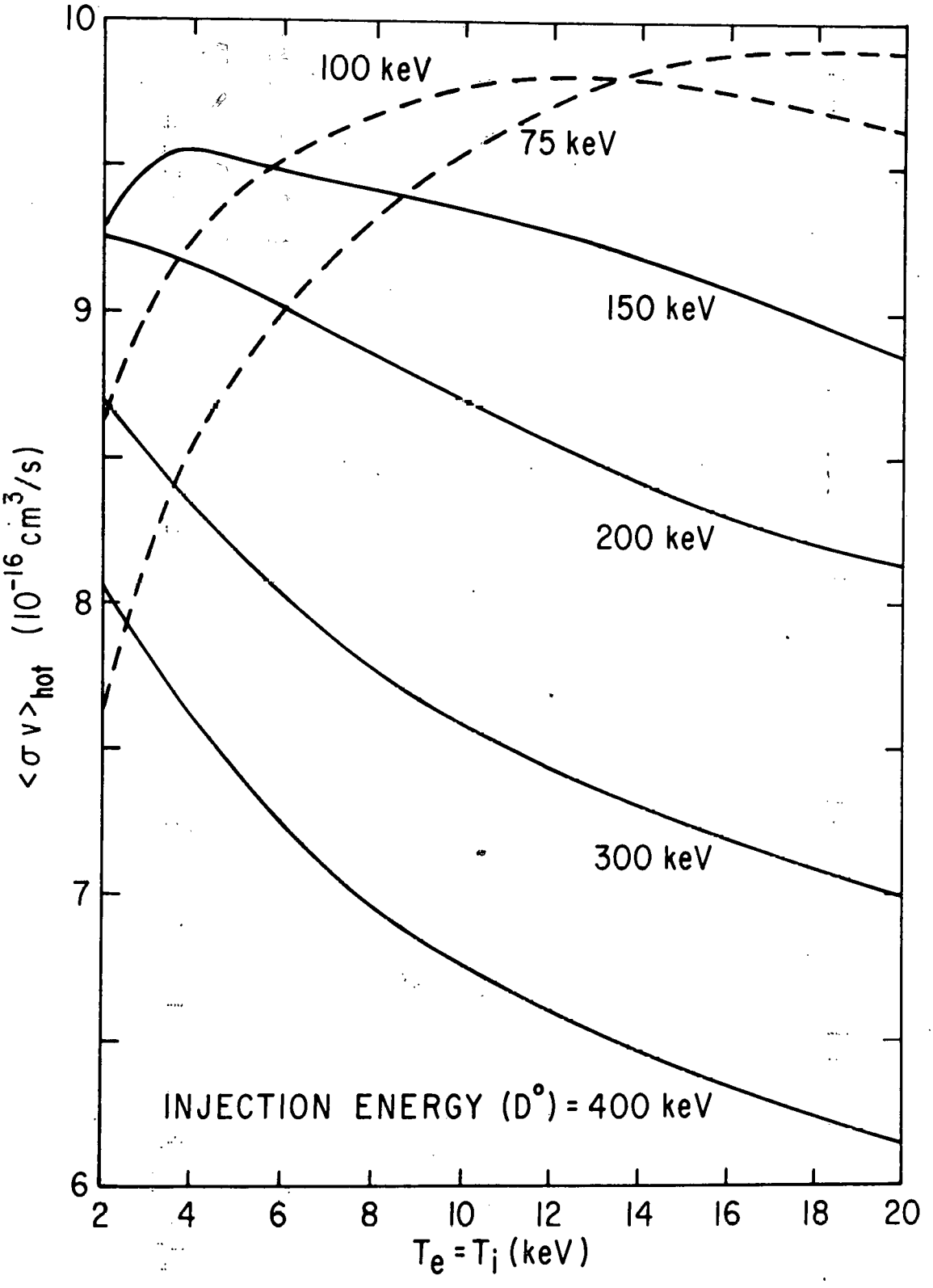


753986

Fig. 4. Fusion reactivity of isotropic, steady-state distributions of deuterons and tritons injected into a 50:50 D-T plasma of temperature $T_e = T_i$. Triton injection energy = 3/2 deuteron injection energy.

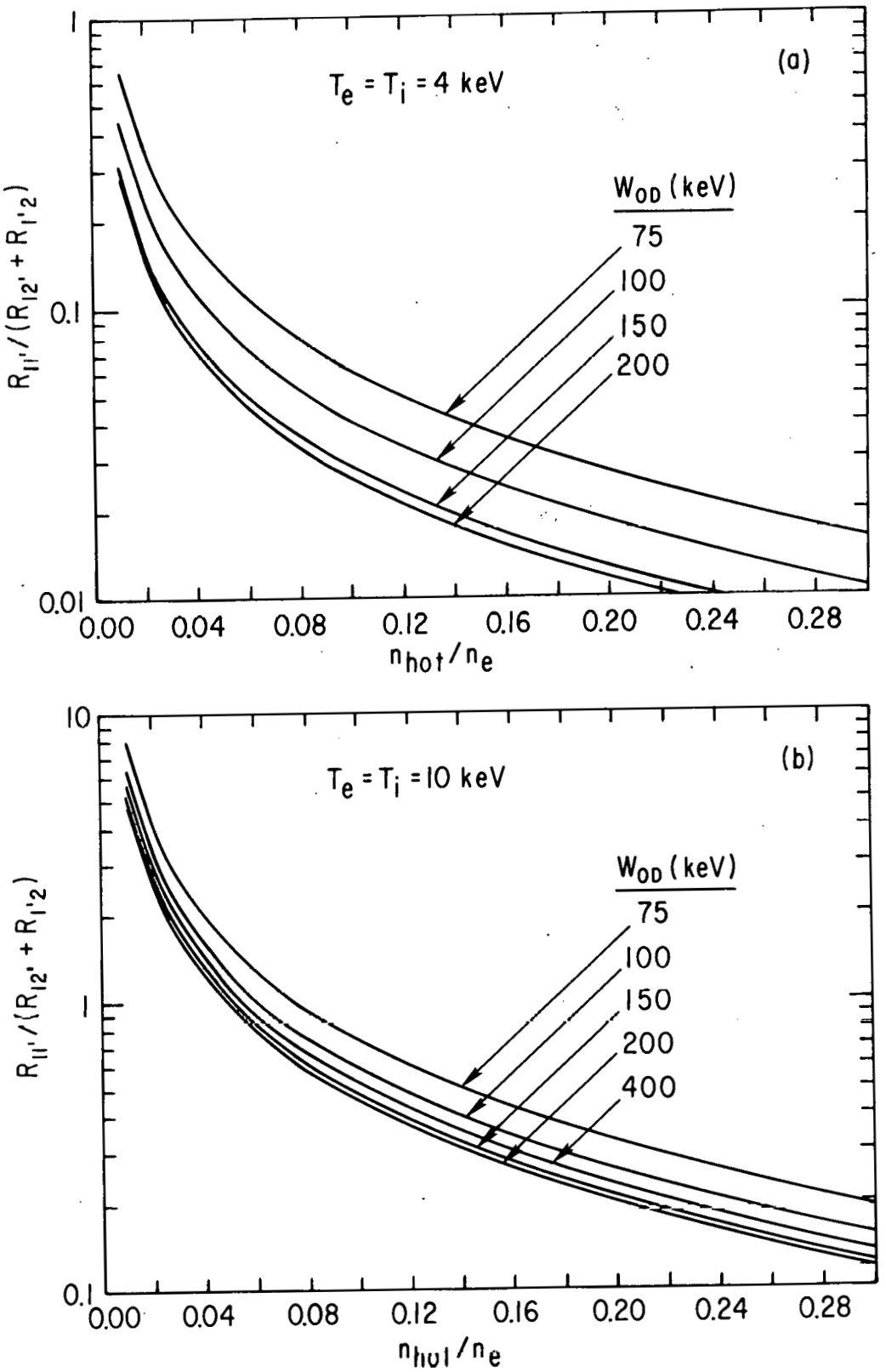


753991

Fig. 5. Ratio of the thermonuclear reaction rate ($R_{11'}$) to the target-plasma reaction rate for a 50:50 D-T plasma with temperature $T_e = T_i$ maintained by injection of deuteron and triton beams of the same intensity and velocity. $n_{hot}$ is the total density of energetic ions.

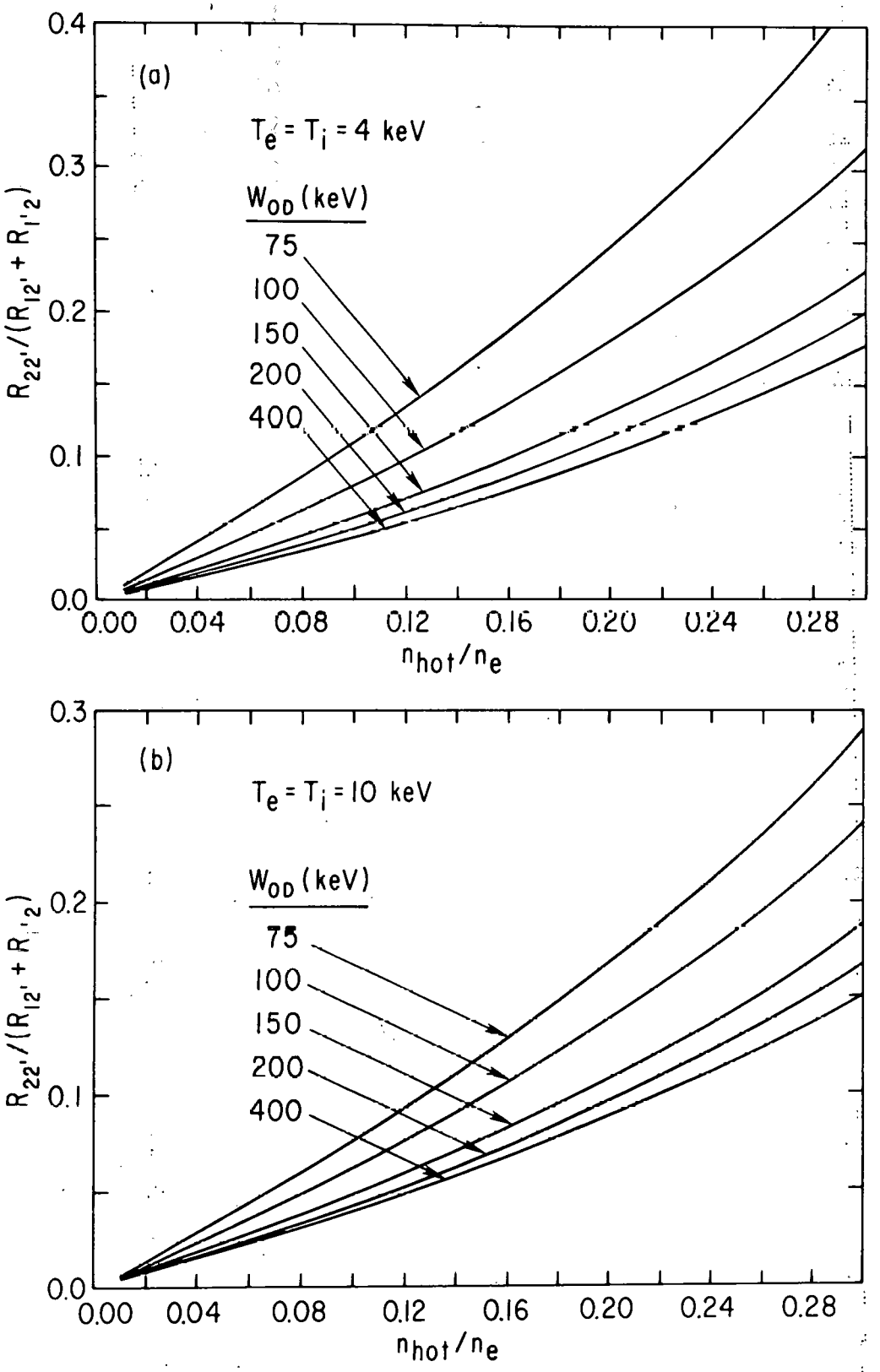


753990

Fig. 6. Ratio of the fusion reaction rate of isotropic energetic deuterons and tritons ($R_{22'}$) to the target-plasma reaction rate for a 50:50 D-T plasma with temperature $T_e = T_i$ maintained by injection of deuteron and triton beams of the same intensity and velocity. $n_{hot}$ is the total density of energetic ions.

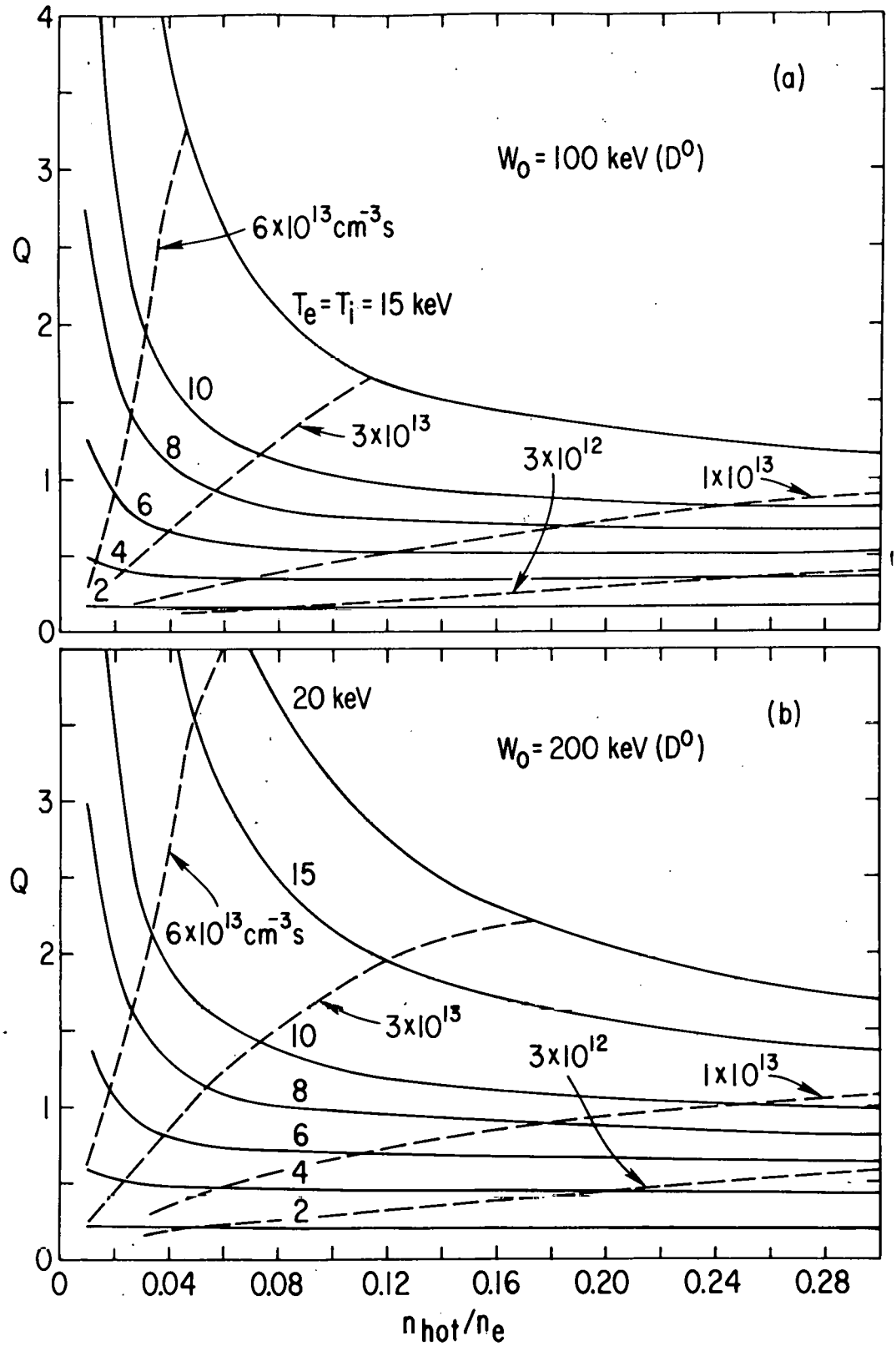


756208

Fig. 7. Fusion power multiplication for 50:50 D-T plasmas at temperature $T_e = T_i$ maintained by injection of energetic deuterons at energy $W_o^i$ and tritons at energy $3/2W_o$. The dashed curves are contours of $n_e \tau_E$. $n_{hot}$ is the total density of energetic ions.

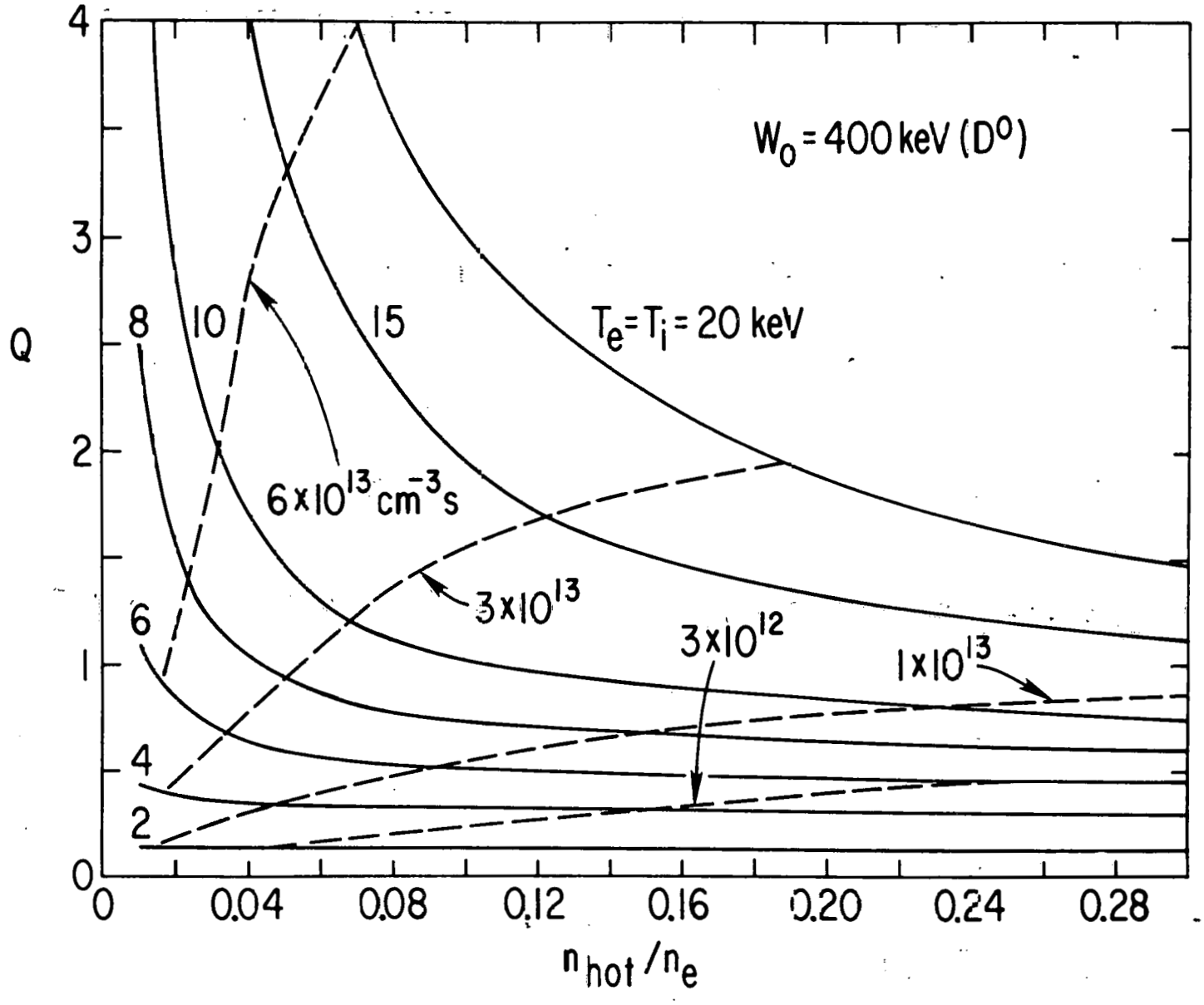


756206

Fig. 8. Fusion power multiplication for 50:50 D-T plasmas at temperature $T_e = T_i$ maintained by injection of 400-keV deuterons and 600-keV tritons. The dashed curves are contours of $n_e\tau_E$. $n_{hot}$ is the total density of energetic ions.

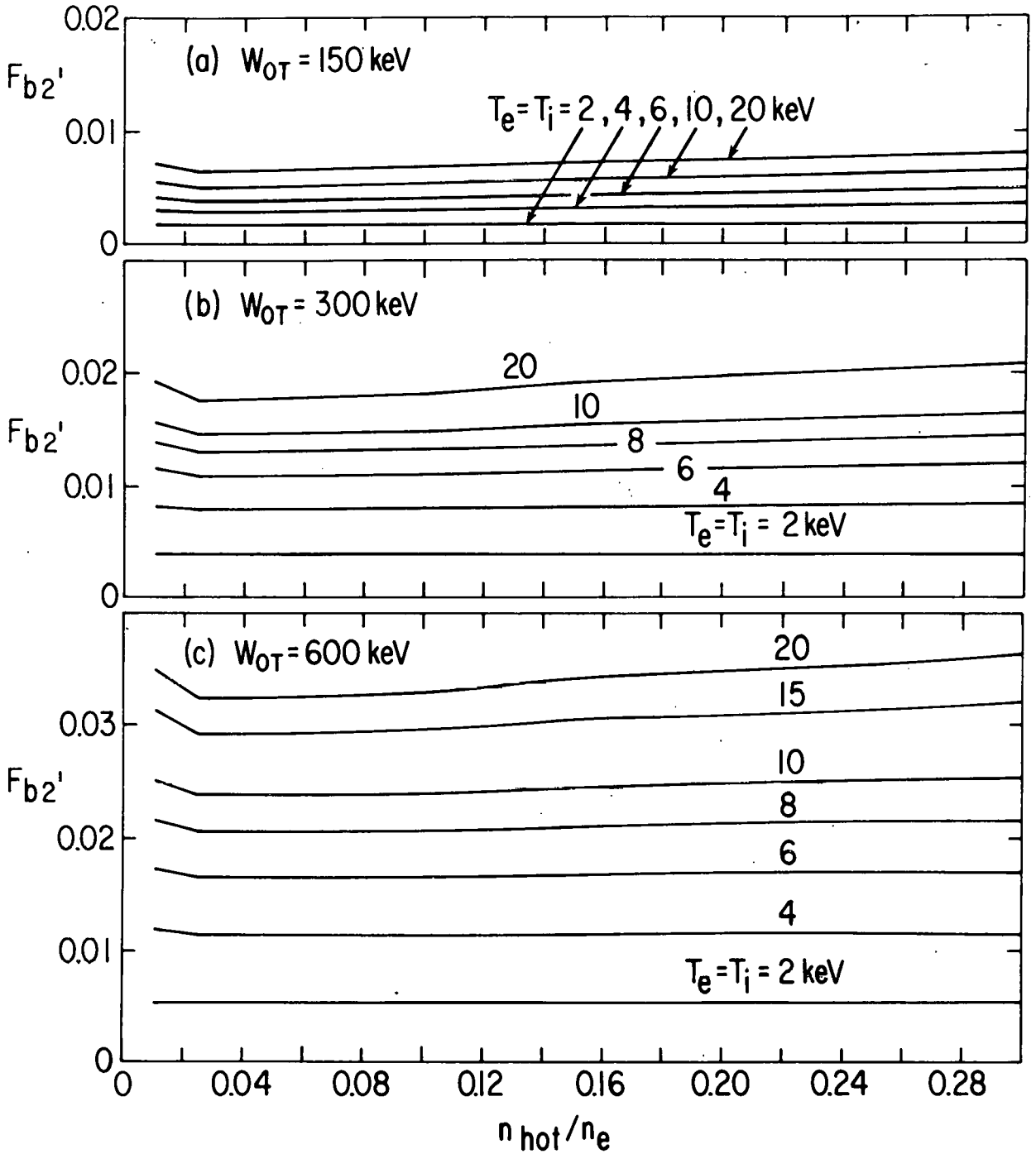


753988

Fig. 9. Fractional burn-up of tritons during deceleration in a 50:50 D-T plasma, after injection at energy $W_{OT}$. Both target-plasma and energetic-ion reactions are taken into account. $n_{hot}$ is the total density of energetic ions.

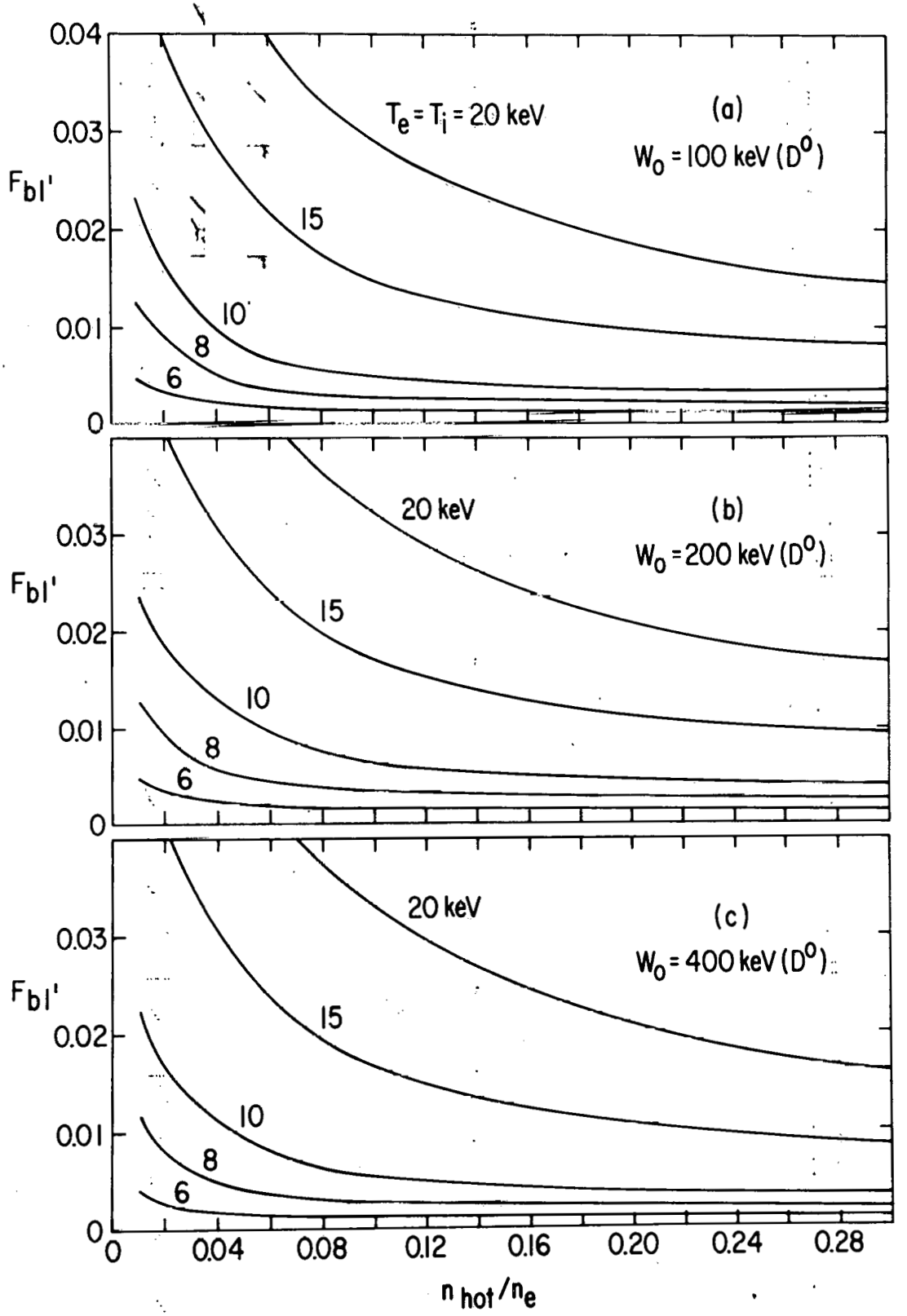


756047

Fig. 10. Fractional burn-up of thermalized tritons during their lifetime in the thermal D-T plasma of temperature $T_e = T_i$.

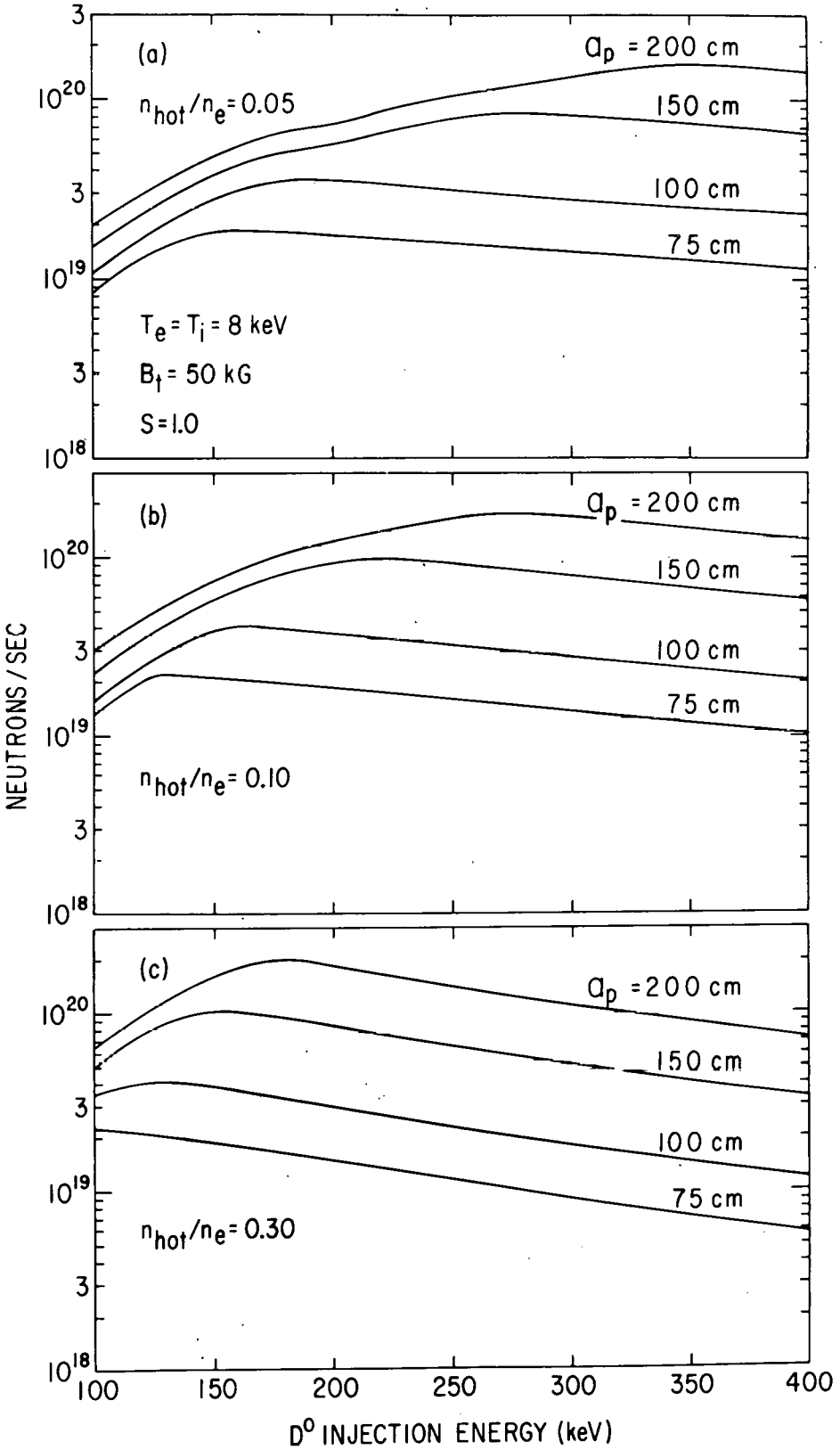


756205

Fig. 11. Variation of neutron production rate with plasma radius and injection energy for 50:50 D-T plasmas of circular cross section maintained at $T_e = T_i = 8$ keV by injection of D and T beams of the same intensity and velocity. Aspect ratio = 4.0.

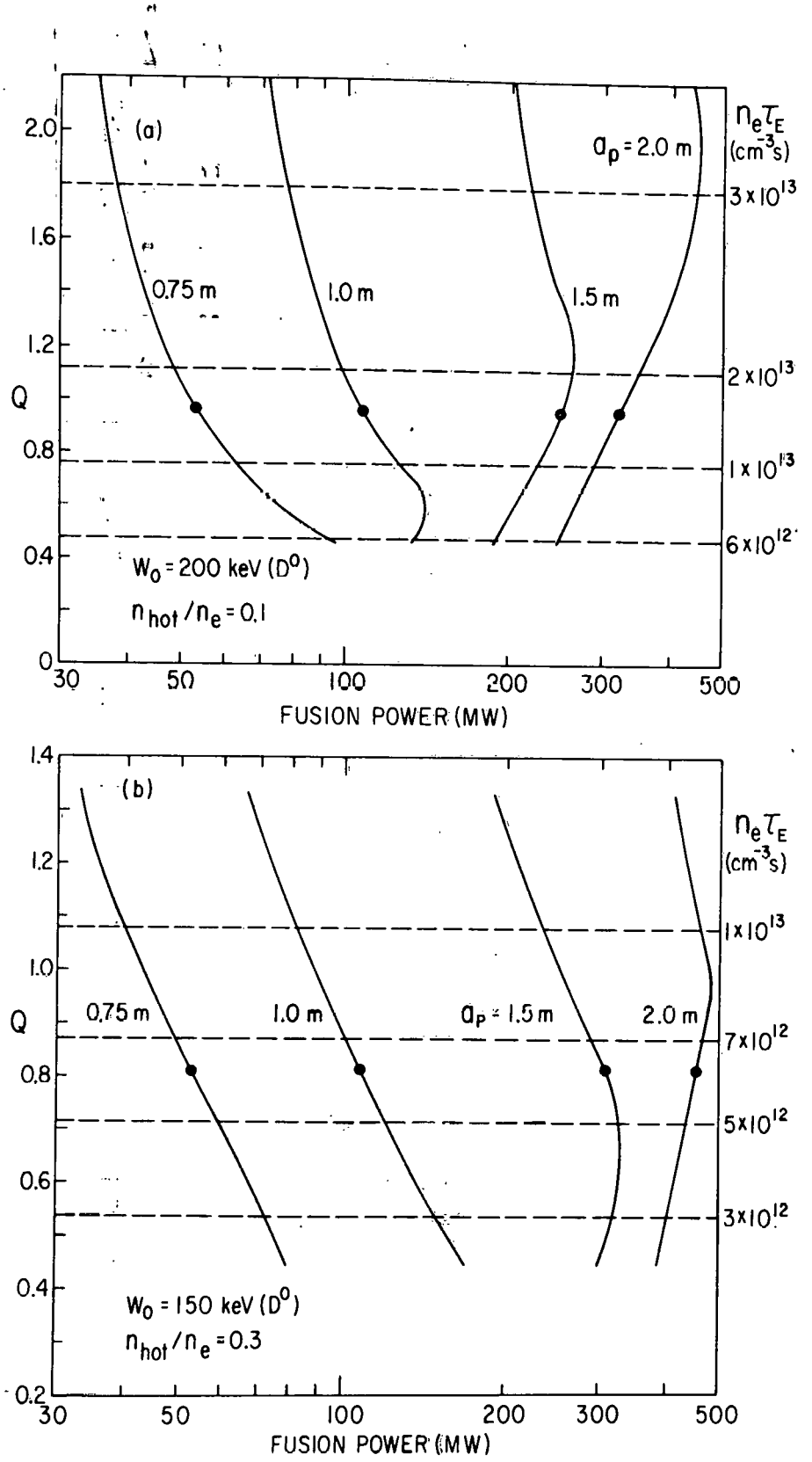


756219

Fig. 12. Fusion power multiplication versus fusion power output for plasmas of radius $a_p$ maintained by injection of D and T beams of the same intensity and velocity. There is a unique relation between $n_e\tau_E$, $T_e$, and Q. The dots denote $T_e = T_i = 8$ keV. Aspect ratio = 4.0.

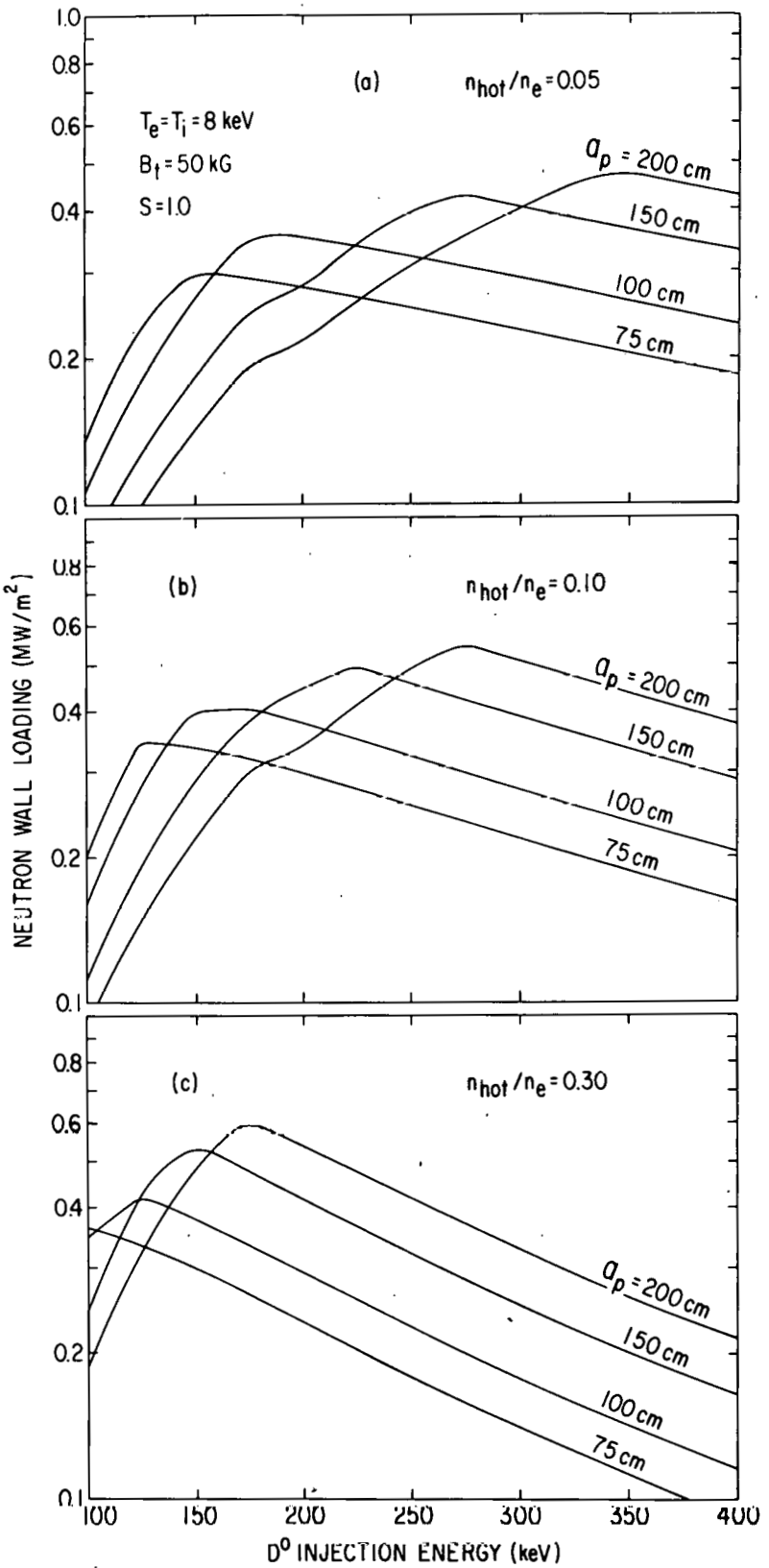


756207

Fig. 13. Variation of neutron wall loading with plasma radius and injection energy for 50:50 D-T plasmas of circular cross section maintained at $T_e = T_i = 8$ keV by injection of D and T beams of the same intensity and velocity. Aspect ratio = 4.0.

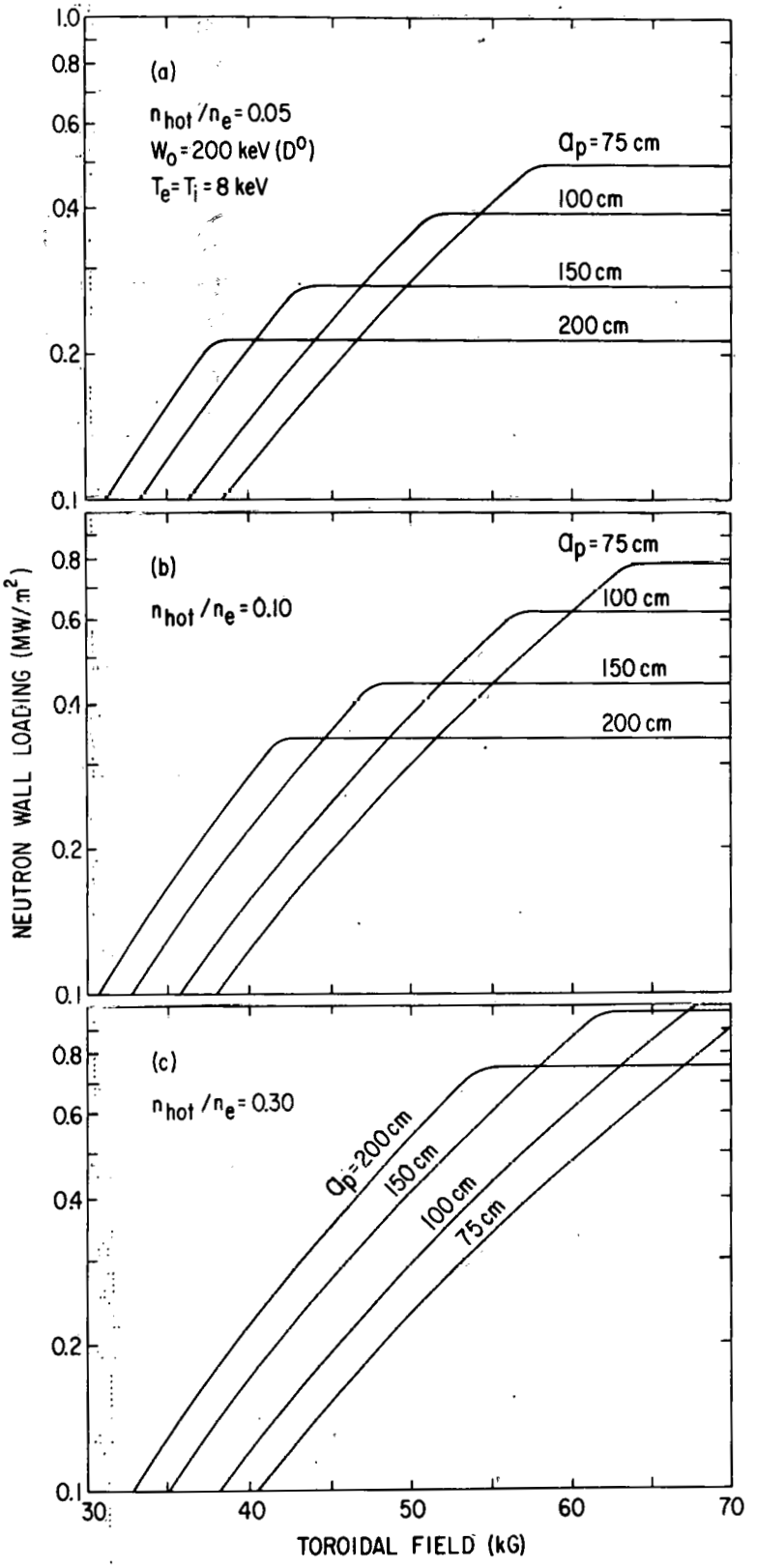


756136

Fig. 14. Variation of neutron wall loading with toroidal field on the magnetic axis. Circular plasmas with aspect ratio = 4.0.

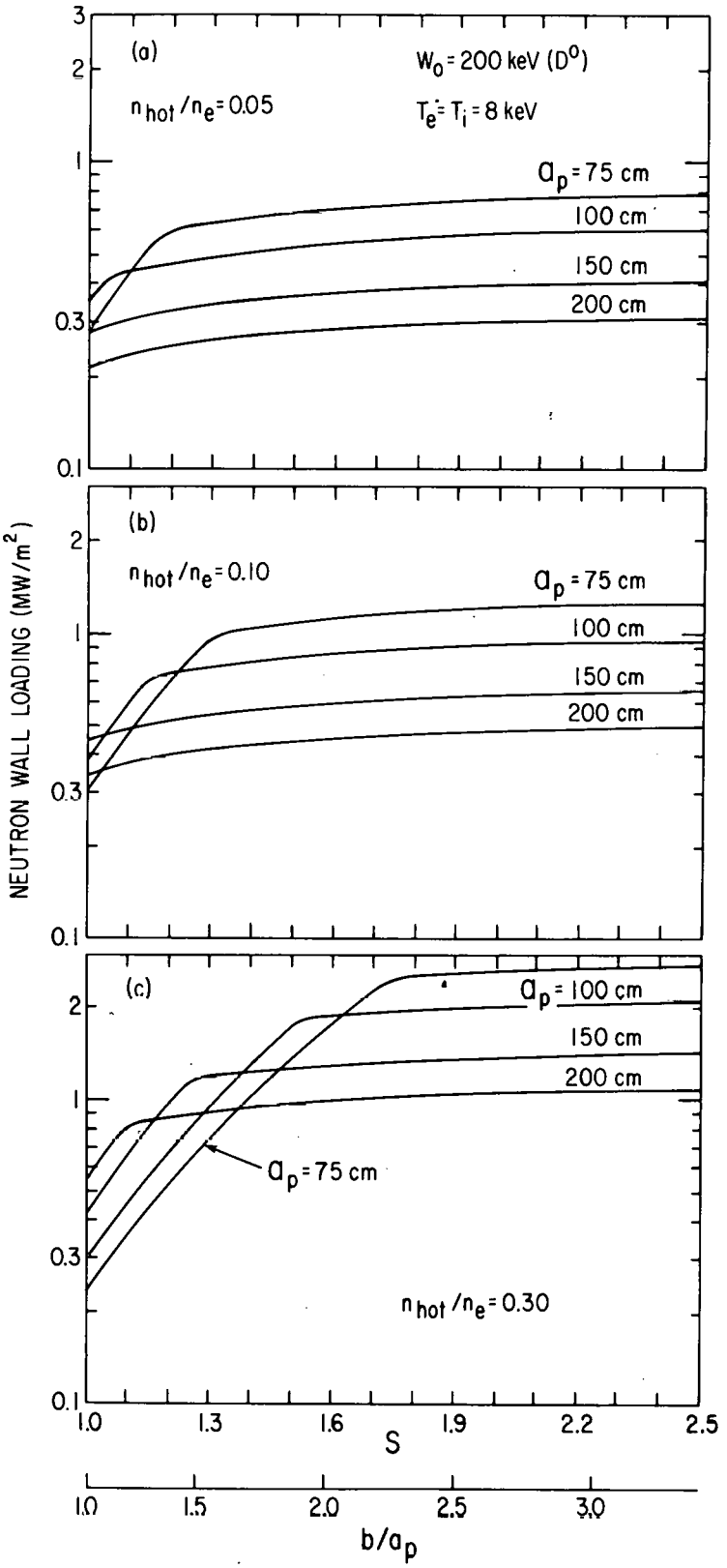


756218

Fig. 15. Variation of neutron wall loading with plasma shape factor S = circumference/$2\pi a_p$. Elliptical plasma with vertical elongation = $b/a_p$. Magnetic field on axis = 50 kG. Aspect ratio = 4.0.

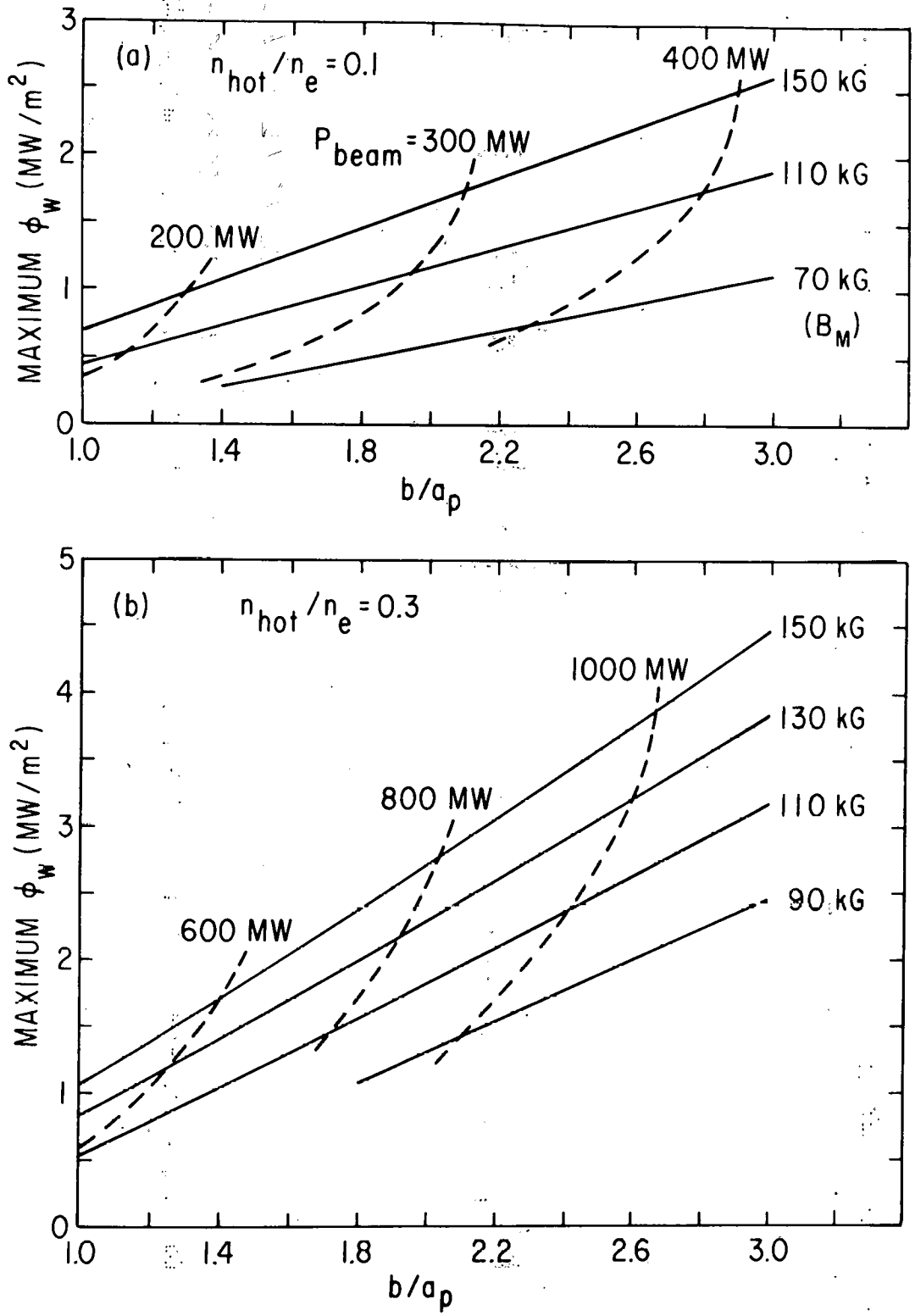


Fig. 16. Maximum neutron wall loading versus plasma vertical elongation ($b/a_p$) and magnetic field at the coil ($B_M$) when the distance from the major axis to the inner edge of the plasma is fixed at 3.1 m. Elliptical plasma with $W_{D^o}$ = 200 keV ($D^o$), 300 keV ($T^o$), $T_e = T_i$ = 8 keV, q = 2.5, $\beta_p$ = 2/3 A. The dashed lines are contours of injected beam power.